Author Manuscript

Author Manuscript

Author Manuscript

Author Manuscript

HHS Public Access

Author manuscript

Cell Chem Biol. Author manuscript; available in PMC 2023 May 19.

Published in final edited form as:

Cell Chem Biol. 2022 May 19; 29(5): 811–823.e7. doi:10.1016/j.chembiol.2022.02.004.

Resurfaced ZIKV EDIII nanoparticle immunogens elicit neutralizing and protective responses *in vivo*

George I. Georgiev[1], **Ryan J. Malonis**[1], **Ariel S. Wirchnianski**[1,2], **Alex W. Wessel**[3], **Helen S. Jung**[1], **Sean M. Cahill**[1], **Elisabeth K. Nyakatura**[1,6], **Olivia Vergnolle**[1,6], **Kimberly A. Dowd**[7], **David Cowburn**[1], **Theodore C. Pierson**[7], **Michael S. Diamond**[3,4,5], **Jonathan R. Lai**[1,8,*]

[1]Department of Biochemistry, New York, NY 10461, USA

[2]Department of Microbiology and Immunology, Albert Einstein College of Medicine, New York, NY 10461, USA

[3]Department of Medicine, Washington University in St. Louis, School of Medicine, St. Louis, MO 63110, USA

[4]Department of Molecular Microbiology, Washington University in St. Louis, School of Medicine, St. Louis, MO 63110, USA

[5]Department of Pathology & Immunology, Washington University in St. Louis, School of Medicine, St. Louis, MO 63110, USA

[6]Present address: Tri-Institutional Therapeutics Discovery Institute, New York, NY 10021, USA

[7]Viral Pathogenesis Section, National Institute of Allergy and Infectious Diseases, National Institutes of Health, Bethesda, MD 20892, USA

[8]Lead Contact

Summary

Zika virus (ZIKV) is a flavivirus that can cause severe disease, but there are no approved treatments or vaccines. A complication for flavivirus vaccine development is the potential of immunogens to enhance infection via antibody-dependent enhancement (ADE), a process mediated by poorly-neutralizing and cross-reactive antibodies. Thus, there is strong rationale to develop immunogens that minimize the potential to elicit enhancing antibodies. Here, we utilized structure-based protein engineering to develop “resurfaced” ZIKV immunogens based on the E glycoprotein domain III (“rsZDIIIs”), in which epitopes bound by variably-neutralizing antibodies were masked by combinatorial mutagenesis. We identified one resurfaced EDIII immunogen (rsZDIII-2.39) that elicited a protective, yet immune-focused response. Compared to

*Correspondence: jon.lai@einsteinmed.edu.

AUTHOR CONTRIBUTIONS

G.I.G., A.S.W., and J.R.L. designed the research; G.I.G., R.J.M., A.S.W., A.W.W., H.J., S.M.C., E.K.N., O.V., K.A.D., D.C., and T.C.P. performed research. G.I.G., A.S.W., A.W.S., S.M.C., E.K.N., O.V., K.A.D., T.C.P., M.S.D., and J.R.L. analyzed data. G.I.G. and J.R.L. wrote the manuscript.

Publisher's Disclaimer: This is a PDF file of an unedited manuscript that has been accepted for publication. As a service to our customers we are providing this early version of the manuscript. The manuscript will undergo copyediting, typesetting, and review of the resulting proof before it is published in its final form. Please note that during the production process errors may be discovered which could affect the content, and all legal disclaimers that apply to the journal pertain.

Author Manuscript Author Manuscript Author Manuscript Author Manuscript

AaLS-ZDIII-WT, immunization with AaLS-rsZDIII-2.39 produced fewer numbers of ZIKV EDIII antigen-reactive B cells, and elicited serum which had a lower magnitude of induced ADE against DENV1. Our findings enhance our understanding of the structural and functional determinants of antibody protection against ZIKV.

eTOC Blurb

Flavivirus vaccine development is complicated by the risk of antibody-dependent enhancement (ADE), which is mediated by non-neutralizing antibodies. *Georgiev et al.* use structure-guided phage display to mask epitopes in the ZIKV EDIII subunit that are targeted by non-neutralizing antibodies. The resurfaced “rsZDIII” immunogens elicit protective yet immune-focused responses in mice.

Graphical Abstract

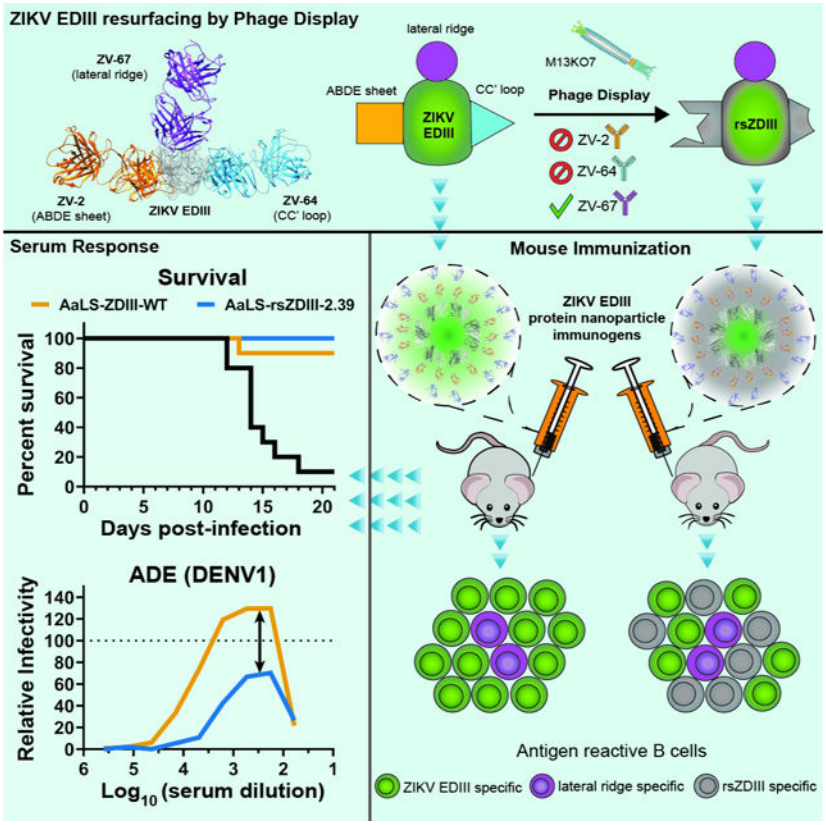

INTRODUCTION

ZIKV, a member of the Flavivirus genus of the *Flaviviridae* family, was first identified in a rhesus monkey in the forests of Uganda in the 1940s, and caused sporadic outbreaks in parts of Africa and Asia though the 20th century (Dick et al., 1952; Heinz and Stiasny, 2017). Major epidemics in Oceania (2007) and the Americas (2015) raised global attention to this emerging pathogen (Duffy et al., 2009; Pierson and Diamond, 2018; Roth et al., 2014). ZIKV and DENV1–4 are transmitted by the same *Aedes* mosquito vectors and

Author Manuscript Author Manuscript Author Manuscript Author Manuscript

have co-circulated in tropical and sub-tropical regions (Heinz and Stiasny, 2017; Lazear and Diamond, 2016; Roth et al., 2014). Infection by ZIKV can be asymptomatic or cause mild clinical symptoms in most adults (Lazear and Diamond, 2016; Pierson and Diamond, 2018); however, in some patients, severe neurological complications including Guillain-Barre syndrome can arise (Cao-Lormeau et al., 2016; Oehler et al., 2013). Infection during pregnancy can have devastating consequences, such as ZIKV-induced congenital ZIKV syndrome (CZS), which results in fetal death or infants born with microcephaly and other congenital anomalies (Brasil et al., 2016; Mlakar et al., 2016; Pierson and Diamond, 2018; Rasmussen et al., 2016). At present there are no approved treatments for ZIKV infection, although several vaccines are currently undergoing clinical testing (Pierson and Graham, 2016; Thomas and Barrett, 2020).

The mature ZIKV virion contains a ~11 kb positive-sense RNA genome, which is encapsidated and surrounded by a lipid membrane displaying 180 copies of the integral envelope (E) glycoprotein. Ninety homodimers of the E-glycoprotein are arranged in herringbone symmetry, covering the surface of the viral particle (Sirohi et al., 2016). During infection, the E protein mediates cell attachment and viral membrane fusion, and is a primary target of neutralizing antibodies (Heinz and Stiasny, 2017). Each E subunit contains three domains, EDI, EDII, and EDIII (Dai et al., 2016). EDII contains the fusion loop; the central EDI domain connects to EDIII, which is anchored via the stem and C-terminal transmembrane domain into the viral membrane. Fusion is driven by E homodimer dissociation and insertion of the fusion loop into the endosome membrane, followed by refolding to adopt a post-fusion trimeric hairpin conformation (Heinz and Stiasny, 2017). The ZIKV EDIII domain (ZDIII-WT), which adopts an Ig-like β-sandwich fold, contains a protective lateral ridge (LR) epitope, which structurally encompasses the region preceding the A strand, as well as the BC-, DE-, and FG-loops. Importantly, the ZIKV EDIII LR epitope is a target for potently neutralizing antibodies, including some that cross-neutralize DENV1 (Robbiani et al., 2017; Sapparapu et al., 2016; Stettler et al., 2016; Zhao et al., 2016). However, other epitopes such as the ABDE-sheet and CC’ loop epitopes of ZIKV EDIII are targeted by non- or less neutralizing antibodies, which might be unfavorable for vaccine development. A recent study with ZIKV EDIII-based immunogens revealed that a substantial antibody response toward the CC’ loop is elicited in non-human primates (Yang et al., 2021).

Development of safe and effective DENV vaccines has proven challenging (Pierson and Graham, 2016; Thomas and Barrett, 2020), as efforts have been complicated by a phenomenon known as antibody-dependent enhancement of infection (ADE) which can exacerbate infection and disease in some DENV-experienced individuals (Halstead, 2003). ADE is caused by antibodies elicited during a primary infection, or by vaccination, that are cross-reactive but poorly neutralizing against other closely related flaviviruses. Upon secondary infection by a heterologous virus, these antibodies can promote uptake of the non-neutralized virus complex into myeloid cells, via Fcγ receptor interactions, and increase viral pathogenesis (Guzman et al., 2013). Consequently, a critical objective for DENV vaccine design is to elicit a broadly neutralizing antibody response, while limiting cross-reactive and weakly neutralizing antibodies that increase risk of ADE. Restricting the

Author Manuscript Author Manuscript Author Manuscript Author Manuscript

antigenic landscape of a vaccine immunogen could limit the risk of eliciting ADE, thus making the 11 kDa EDIII domain an attractive subunit vaccine candidate.

Recent epidemiological studies suggest that pre-existing ZIKV immunity may enhance disease severity upon subsequent infection with some DENV serotypes in humans (Katzelnick et al., 2020b), and similar conclusions have been drawn from sequential immunization or infection experiments in mice and primates (Katzelnick et al., 2020a). In contrast, the risk of ZIKV infection appears to be reduced in DENV-experienced individuals (Andrade et al., 2019). The potential for heterotypic ADE induced by ZIKV vaccines suggests that immunogens containing fewer epitopes that are targeted by non- or poorly neutralizing, and especially cross-reactive antibodies, would be advantageous.

In this work we used structure-guided protein design and phage display to engineer resurfaced rsZDIII immunogens where the LR epitope, which is engaged by protective antibodies, is maintained but regions of the ABDE sheet and CC' loop, which are bound by non- or variably-neutralizing antibodies, are masked by mutations leading to amino acid substitution. We hypothesized rsZDIIIs could elicit protective responses directed at the LR, but with fewer reactive B cells toward ABDE sheet or CC' loop epitopes. The engineered rsZDIIIs bound strongly to a protective LR mAb (ZV-67), but showed reduced binding to ABDE sheet and CC' loop mAbs, ZV-2 and ZV-64 respectively. We examined the capacity of rsZDIIIs to elicit a neutralizing antibody response when mounted onto protein-based nanoparticles, and found that one rsZDIII nanoparticle (AaLS-ZDIII-2.39) elicited potently neutralizing and protective responses in mice. Furthermore, profiling of $CD19^{+}$/ IgG^{+} splenocytes revealed that even though the neutralizing antibody titers of AaLS-rsZDIII-2.39 and AaLS-ZDIII-WT immunized mice were similar, the frequency of ZDIII-WT antigen-reactive B cells was lower in mice that received the rsZDIII-based immunogen. These results provide a roadmap for development of future resurfaced flavivirus EDIII vaccines.

RESULTS

Isolation of resurfaced ZIKV-EDIII variants (rsZDIIIs) by phage display.

ZIKV EDIII (ZDIII-WT) is a target of protective neutralizing mAbs isolated from natural human or mouse infections (Robbiani et al., 2017; Rogers et al., 2017; Stettler et al., 2016; Zhao et al., 2016). Most human ZIKV EDIII mAbs do not cross-react with DENV EDIII with the exception of Z004, Z006, and ZIKV-116, which bind the LR epitope and cross-neutralize DENV1 but none of the other DENV serotypes (Robbiani et al., 2017; Sapparapu et al., 2016). The LR epitope encompasses residues at the N-terminus and the BC-, DE-, and FG-loops, but the cross-reactive region targeted by Z004 and Z006 is localized to E393 and K394 of the FG-loop (ZIKV numbering; E384/K385 in DENV) (Nybakken et al., 2005). Aside from these few mAbs binding this small epitope, most other ZIKV EDIII directed mAbs do not cross-react with DENV EDIIIs, in contrast to ZIKV mAbs targeting other E epitopes. Thus, EDIII-directed immunogens are unlikely to elicit ADE responses between DENV and ZIKV.

Our rsZDIII engineering approach was informed by structural data for a murine protective antibody (ZV-67), which targets the LR epitope, as well as two non-neutralizing antibodies

Author Manuscript Author Manuscript Author Manuscript Author Manuscript

(ZV-2 and ZV-64), which bind the unfavorable ABDE-sheet and CC'-loop regions of ZIKV DIII, respectively (Figure 1A). We hypothesized that a combinatorial "resurfacing" strategy would yield rsZDIIIs that maintained the neutralizing LR epitope, but masked unfavorable ABDE sheet and CC' loop epitopes by mutation. We cloned the ZDIII-WT (H/PF/2013 strain, residues G302-K409, Table S1) as a fusion to the minor coat protein pIII of the M13 bacteriophage as previously reported (Frei and Lai, 2016; Frei et al., 2018); the construct contains an N-terminal FLAG tag for detection of display. Phage ELISA indicated that these phage particles reacted strongly with immobilized ZV-67, ZV-64, ZV-2, and an anti-FLAG antibody M2, but not BSA confirming that ZDIII-WT was expressed efficiently and in a conformationally relevant manner on the phage surface (Figure S1).

We next identified critical contacts in the ABDE sheet (orange spheres) and CC' loop (blue spheres) epitopes for binding to non-neutralizing mAbs ZV-2 and ZV-64 respectively, and targeted those positions for combinatorial mutagenesis (Figure 1B). The ABDE sheet epitope includes positions from multiple secondary structural elements whereas the CC' loop is comprised of contiguous residues from P348 to P354. We utilized a limited diversity randomization scheme where each position was allowed to vary between WT and Alanine (Ala), and a 3rd or 4th residue in some cases due to the degeneracy of the genetic code (see Key Resources Table). We reasoned that such a randomization scheme would result in ZIKV EDIII variants with a high proportion of Ala substitutions in the ABDE sheet and CC' loop. Alanine has a relatively short side chain and is unable to participate in long-range interactions that are critical for high-affinity antibody-antigen interfaces, and is generally under-represented in antibody epitopes (Kringelum et al., 2013). We hypothesized that rsZDIIIs bearing multiple alanine substitutions in the ABDE sheet and CC' loop would not elicit strongly-binding ZV-2 or ZV-64-like antibodies. We subjected the phage library to an initial round of positive selection against mAb ZV-67, to enrich for clones that maintain an intact lateral ridge epitope. After expanding the output phage population, we performed a round of negative selection against mAbs ZV-2 and ZV-64, followed by a second round of positive selection against mAb ZV-67. This selection strategy favored EDIII variants that retained the LR ridge epitope (and thus bound ZV-67) but had significantly remodeled ABDE sheet and CC' loop regions that resulted in attenuated binding to ZV-2 and ZV-64.

Preliminary screening of phage clones from the selection revealed a number of rsZDIIIs with multiple substitutions in the ABDE sheet and CC' loop that maintained strong reactivity toward ZV-67, but that had significantly diminished reactivity toward ZV-2 (Figure 1C shows a representative set). A number of clones retained complete or partial reactivity toward ZV-64 (*e.g.*, rsZDIII-1.39, −1.48, −1.74, −2.16, −2.20, −2.50), whereas others were not reactive at all. In contrast, ZDIII-WT phage exhibited strong reactivity toward all three mAbs. None of the clones in this panel had cross-reactivity toward wells coated with BSA, suggesting that resurfacing did not result in introduction of protein surfaces that are more prone to non-specific interaction. Furthermore, most clones in the panel showed strong reactivity toward M2, an anti-FLAG antibody, indicating high levels of rsZDIII expression on the phage surface. Based on screening reactivity profiles, 14 of the clones were chosen for further testing in a full phage titration ELISA experiment (Figure S1), to determine if relative differences existed in their half-maximal binding phage titer (EC_{50}, Figure 1D). We found that ZDIII-WT phage reacted with all three mAbs with EC_{50} titers of ~10^{6-7}

Author Manuscript Author Manuscript Author Manuscript Author Manuscript

infectious units (IU)/ mL. Most of the resurfaced variants identified maintained this level of reactivity toward ZV-67 (LR mAb) but were 10^1– to 10^7-fold less reactive toward ZV-2 or ZV-64.

Sequence analysis of a subset of clones bearing favorable reactivity profiles revealed a high level of substitution at T315-I317, T327, M375 (ABDE sheet) and Q350, T351, T353 (CC' loop) (Figure 1E). Positions E329, D348, and K373 had less variation, and position E377 maintained WT residue identity in all identified clones. As per the randomization scheme, there was a high proportion of WT⟶Ala mutations, but other side chains also were observed where permitted. Collectively, these results indicate that rsZDIIIs contain altered surface characteristics in the ABDE sheet and CC' loop, but maintain a conformationally relevant LR epitope.

Expression and biochemical characterization of purified rsZDIIIs.

We expressed the ZDIII-WT and those rsZDIIIs with favorable reactivity profiles (clones 1.8, 1.20, 1.39, 1.69, 2.16, and 2.39) as protein fusions to Maltose Binding Protein (MBP) to facilitate recombinant production (Figure 2A). This MBP fusion strategy stabilizes proteins, allows for cytosolic expression, and has been used previously to express soluble flavivirus EDIII (Mukherjee et al., 2006; Watterson et al., 2012). Inclusion of a TEV cleavage site in the linker after MBP allowed for release of the monomeric ZDIII-WT or rsZDIIIs. An additional anion exchange chromatography step was performed to obtain highly homogeneous EDIII protein preparations at the expected molecular size of 13–14 kDa (Figure 2B, Figure S2).

We assessed the binding profiles of purified rsZDIIIs to mAbs ZV-2, ZV-64, and ZV-67 by ELISA (Figures 2C–D, Figure S3A). We observed similar binding profiles for ZV-67, which engages the protective LR epitope, against the ZDIII-WT and rsZDIIIs with half maximal effective concentrations values (EC_{50}) of 14 nM (WT) and 12– 62 nM (rsZDIIIs), respectively. Conversely, binding of ZV-2 and ZV-64, whose epitopes were resurfaced, was attenuated to rsZDIIIs (>100 nM) compared to ZDIII-WT. Taken together, the reactivity profiles observed for the purified proteins closely resemble those seen from full-curve phage ELISAs. Subsequent immunogenicity studies (see below) identified rsZDIII-2.39 as the most promising candidate and thus we further characterized binding interactions by biolayer interferometry. We observed an apparent equilibrium dissociation constant (K_D^{app}) of 16.3 ± 0.2 nM for ZV-67 binding to rsZDIII-2.39, whereas ZV-64 and ZV-2 did not show appreciable binding (Figure 3A). Because these experiments were performed with bivalent IgG antibodies, we cannot rule out the possibility of avidity effects, but the K_D^{app} values nonetheless can be used for comparative analysis. In contrast, all three mAbs (ZV-2, ZV-64, and ZV-67) engaged ZDIII-WT with K_D^{app} values of 10.7 ± 0.09 nM, 43.2 ± 0.7 nM, and 43 ± 1.1 nM, respectively, that were in reasonable agreement with previous reports (Zhao et al., 2016).

To determine whether the mutations in resurfaced rsZDIII-2.39 altered the core EDIII fold, we generated an ^{15}N-labeled version and obtained ^1H-^{15}N heteronuclear single quantum coherence (HSQC) spectra (Figure 3B) under conditions that were similar to those previously reported for ZDIII-WT (Wang et al., 2017). Comparison of fingerprint regions

Author Manuscript Author Manuscript Author Manuscript Author Manuscript

from acquired rsZDIII-2.39 spectra and deposited ZDIII-WT spectra revealed significant chemical shift overlap in core residues (Figure 3C, Figure S4), suggesting that resurfacing of the ABDE and CC' loop epitopes did not substantively disrupt the structure of the rsZDIII-2.39 relative to ZDIII-WT (Table S2). Taken together, these results indicate that the resurfacing of the ABDE-sheet and CC' loop epitopes in rsZDIIIs attenuates binding of non-neutralizing antibodies but does not compromise the structural integrity of the EDIII fold.

Generation and immunogenicity of *Aquifex aeolicus* lumazine synthase (AaLS) nanoparticles that multivalently present rsZDIIIs.

We previously described immunogenicity studies with resurfaced EDIII variants based on DENV2 (rsDIII-Ala30) (Frei et al., 2018), which elicited a broadly reactive and cross-neutralizing response *in vitro*. While rsDIII-Ala30 sera neutralized DENV1–3, this neutralizing breadth did not extend to DENV4 and the sera were not sufficiently potent to protect mice from lethal DENV2 challenge when passively transferred. The neutralizing potency of the response may have been limited due to the inherent nature of the monomeric EDIII-based antigens, as small protein and peptide immunogens have a short serum half-life *in vivo*, and are inefficient at cross-linking B cell receptors (BCRs) that promote B cell survival and antibody maturation. To mitigate these issues, rsZDIIIs were displayed multivalently on protein nanoparticles which we hypothesized would stimulate the humoral response and boost neutralizing titers.

Lumazine synthase from *Aquifex aeolicus* (AaLS) is an enzyme involved in riboflavin biosynthesis that naturally assembles into a stable 60-mer nanoparticle.[5] Antigen-AaLS conjugates or fusions have been explored as potential vaccines for a number of viruses, and the pathogen-like display of the immunogen on the AaLS nanoparticle make it an attractive choice for presentation of the rsZDIIIs in a multivalent form (Ladenstein and Morgunova, 2020). We used the Spycatcher (SpyC)/Spytag (SpyT) bio-conjugation system (Sun et al., 2014; Zakeri et al., 2012) to covalently link rsZDIIIs to the AaLS monomers (Figure 4A). The 151-residue protein CnaB2 contains a natural isopeptide bond that can be reconstituted as two polypeptides; the "Spytag" (SpyT) is a 13-residue peptide corresponding to the C-terminal β-strand of CnaB that spontaneously forms an isopeptide bond to its protein partner, Spycatcher (SpyC), which consists of the remainder of the domain. AaLS was engineered with a C-terminal SpyC fusion (AaLS-SpyC) and a C-terminal SpyT incorporated into rsZDIIIs (rsZDIII-SpyT). Mixture of AaLS-SpyC with a 4-fold molar excess of rsZDIII-SpyT resulted in conjugation of the AaLS-SpyC monomer to yield AaLS-rsZDIII within 16 hours (Figure 4B, AaLS-rsZDIII-2.39 shown as an example). AaLS-rsZDIII nanoparticles were prepared for rsZDIII clones 1.20, 1.39, 2.16, 2.39. Clone 1.69 had low expression yield and clone 1.8 was prone to aggregation, and thus these two rsZDIIIs were not further evaluated. We assessed the size and morphology of the AaLS-rsZDIII-2.39 preparation by negative stain electron microscopy, and observed monodisperse spherical particles of ~20 nm in diameter as expected based on previous studies with AaLS nanoparticles (Ladenstein and Morgunova, 2020) (Figure 4C).

Author Manuscript Author Manuscript Author Manuscript Author Manuscript

We evaluated the capacity of AaLS-rsZDIIIs to induce neutralizing antibody responses by immunizing groups of 6- to 8-week-old female BALB/c mice (n=5–10) by intraperitoneal (i.p.) injection with three doses of 15 μg AaLS-rsZDIIIs, spaced 3 weeks apart, using Addavax adjuvant (Figure 4D). A control group, receiving a weight-adjusted molar equivalent dose (5 μg) of monomeric rsZDIII-2.39 was included to compare the nanoparticle-presented antigen to a monomeric version. Serum samples were collected two weeks following booster injections, at days 35 and 56 (D35 and D56, respectively), and characterized by ELISA for IgG responses toward the respective rsZDIII immunogen (Figure 4E). We observed robust induction of immunogen-specific IgG antibodies by all AaLS-rsZDIIIs tested, as well as monomeric rsZDIII-2.39, with mean half-maximal (EC_{50}) binding titers ranging from 1: 4,000 and 1:164,000 on D56. For all groups, there was no statistically significant difference in antibody titers after two (D35) or three (D56) doses. Interestingly, multimeric EDIII presentation did not appear to affect reactive IgG binding titers, with no difference seen in the elicited response to monomeric or AaLS-conjugated rsZDIII-2.39 (Figure 4E).

AaLS-ZDIII WT and AaLS-rsZDIII-2.39 nanoparticle immunization groups showed the greatest neutralization capacity, with mean half-maximal neutralization titers ($FRNT_{50}$) of 1:2,680 and 1:6,100 respectively (Figure 4F). Consistent with the results for serum antibody binding titers, there was no significant difference in neutralization titers in sera obtained at D35 and D56 (Figure S5). Whereas immunization with monomeric rsZDIII-2.39 or AaLS-rsZDIII-2.39 resulted in similar titers of reactive IgG antibodies (Figure 4E), a significant difference was observed in their neutralizing activity. Sera from animals vaccinated with AaLS-rsZDIII-2.39 nanoparticles showed approximately 50-fold greater neutralizing titers against ZIKV than monomeric rsZDIII-2.39 (Figure 4F). This finding suggests that binding is necessary but not sufficient for effective virus neutralization. Furthermore, the manner in which these immunogens are presented to the immune system affects the nature of antibodies elicited, with multivalent nanoparticle presentation eliciting a stronger inhibitory response.

Other AaLS-rsZDIII variants elicited neutralizing but less potent responses, despite exhibiting similar mAb reactivity profiles to rsZDIII-2.39 *in vitro*. Given the close phylogenetic relationship of ZIKV to the DENV serocluster, we assessed potential cross-reactivity of sera elicited by AaLS-rsZDIII-2.39 and AaLS-ZDIII-WT toward DENV1–4 EDIIIs (Figure 4G). Only weak to moderate cross-reactivity was observed toward DENV EDIIIs (median titers of 1:148 – 1:1282), which was significantly less than serum reactivity toward ZIKV EDIII. To explore whether these immunogens elicited antibodies that induce heterotypic ADE, we tested sera from AaLS-ZDIII-WT and AaLS-rsZDIII-2.39 immunized mice (sera from mice in each group were pooled separately) for enhancement of infection of FcγR IIA^+ K562 erythroleukemic cells with reporter virus particles (RVPs) bearing prM-E from DENV1, 2, and 4 (Figure 5) (Pierson et al., 2007). None of the sera induced ADE for DENV2 or 4. However, modest levels of ADE were observed for DENV1, likely reflecting the closer phylogenetic relationship to ZIKV. The overall magnitude of enhancement at the peak enhancement titer was lower for AaLS-ZDIII-2.39 than AaLS-ZDIII-WT, indicating that, while enhancing antibodies exist in both samples, there are fewer in mice immunized with AaLS-ZDIII-2.39.

Author Manuscript Author Manuscript Author Manuscript Author Manuscript

AaLS-ZDIII-WT and AaLS-rsZDIII-2.39 antisera protect mice from lethal ZIKV challenge, but the nature of the elicited B cell populations vary.

We evaluated the potential of the D56 sera from AaLS-ZDIII-WT and AaLS-rsZDIII-2.39 immunized groups to protect mice against lethal ZIKV challenge by passive serum transfer (Figure 6A). One day prior to virus inoculation, 9- to 10-week old male C57BL/6J mice were administered 100 μL of D56 immune serum and a single dose of anti-Ifnar1 antibody (clone MAR1–5A3) to facilitate a lethal challenge model (Lazear et al., 2016). The following day, mice were inoculated by subcutaneous injection with 3×10^5 focus-forming units (FFUs) of a heterologous, African lineage ZIKV (strain Dakar 41525) and observed for weight loss and lethality over time. We observed protection against weight loss and death in mice administered serum elicited by AaLS-rsZDIII-2.39 (Figures 6B–C), compared to serum from an AaLS control group, which showed 10% survival ($p<0.001$). Animals injected with serum elicited by AaLS-ZDIII-WT also showed high levels of protection (90%), which was not statistically different from results seen in the AaLS-rsZDIII-2.39 group, but showed a higher range of weight change for animals within the immunization group (Figure 6C). Additional studies with lower doses of serum and characterization of the viral load during the challenge would be required to fully establish differences in protective activity.

To evaluate the effect of resurfacing the ZDIII-WT immunogen on the elicited immune response, we assessed the population of antigen-reactive splenic B cells from vaccinated animals at D56 by flow cytometry. Gating on $CD19^+/IgG^+$ B cells and using a biotinylated ZDIII-WT probe (see Figure S6 for gating scheme and primary data), we observed fewer ZDIII-WT-reactive B cells in AaLS-rsZDIII-2.39 samples (0.077%), compared to the AaLS-ZDIII-WT group (0.13%) (Figures 6D–E). This finding supports the hypothesis that resurfacing the targeted ABDE-sheet and CC’ loop epitopes by mutagenesis altered these regions sufficiently to elicit an immune focused ZDIII-WT-reactive B cell population.

DISCUSSION

We describe structure-based design of resurfaced ZIKV EDIII immunogens that maintain the LR epitope, but contain significantly remodeled ABDE sheet and CC’ loop regions. While many rsZDIIIs were indistinguishable from one another in their reactivity profiles toward ZV-2, ZV-64, and ZV-67, immunogenicity studies revealed a broad range of neutralization potencies in response to immunization with different AaLS-rsZDIII nanoparticles. Given that overall binding titers among sera against the rsZDIIIs were similar, the differences in neutralizing titer likely are due to varying amounts of antibody directed toward the neutralizing LR epitope. This result is somewhat unexpected given the overall similarity in the sequence of the rsZDIII clones, and likely cannot be explained by antigen trafficking or processing, given that they were all administered with the same adjuvant and presented on the same AaLS nanoparticle platform. One possibility is that rsZDIII-2.39 was the most structurally similar to ZDIII-WT, and thus most similar in its ability to elicit neutralizing antibody against conformational epitopes such as the LR. Further NMR experiments with other rsZDIII variants would be required to confirm this hypothesis.

Author Manuscript Author Manuscript Author Manuscript Author Manuscript

The most promising candidate, AaLS-rsZDIII-2.39, elicited a neutralizing and protective antibody response that was similar to AaLS-ZDIII-WT, but immune profiling revealed that there were significantly fewer ZDIII-WT-reactive splenic B cells in AaLS-rsZDIII-2.39-immunized mice compared to those receiving AaLS-ZDIII-WT-immunizations. This difference is most likely due to fewer B cells reactive to the ABDE sheet and CC' loop, since biochemical studies indicated the reactivity of rsZDIII-2.39 toward ZV-67, as well as the overall fold of the lateral ridge epitope was identical to ZDIII-WT. These results, along with the observed spectrum of neutralizing responses among the rsZDIIIs suggests that fine sequence modifications can substantially impact elicited immune responses. However, in this case, the precise modifications that lead to high neutralizing titers could not be predicted based on binding experiments alone. Therefore, future efforts on resurfaced antigens for ZIKV or other flaviviruses will require a combination of structural design as well as empirical testing *in vivo*.

Comparison of AaLS-rsZDIII-2.39 and monomeric rsZDIII-2.39 antisera demonstrates that antigen presentation, in the context of multivalent nanoparticles, can lead to improved neutralizing titers. However, the binding IgG titers for mice receiving monomeric or AaLS-presented rsZDIII-2.39 were equivalent, and thus in this case nanoparticle presentation resulted in higher amounts of elicited neutralizing antibodies but not necessarily overall reactive immunoglobulins. Previous studies have demonstrated that nanoparticle immunogens are trafficked to germinal centers (Havenar-Daughton et al., 2019; Tokatlian et al., 2019), a critical location for antibody maturation. The larger physical size of the nanoparticle and multivalent presentation likely afford a greater half-life and more efficient cross-linking of B cells (Brouwer et al., 2019; Moyer et al., 2016). The orientation of the antigen presentation on the nanoparticle surface also could play a role, as some regions of the rsZDIII molecule may be physically blocked by the nanoparticle and thus inaccessible to immune cells (Irvine and Read, 2020).

EDIII-based immunogens (monomeric as well as multivalent) have previously been explored as ZIKV vaccines. In most studies, EDIII-based vaccines elicited relatively low neutralizing titers in mice, although in some cases these were sufficient to protect against ZIKV-induced mortality, viral dissemination, or placental infection (Cabral-Miranda et al., 2019; Lin et al., 2019; Tai et al., 2019; Wang et al., 2019; Yang et al., 2021). We note that neutralizing titers elicited by AaLS-ZDIII-WT were stronger than previously reported ZIKV EDIII constructs. Additionally, a ZIKV EDIII variant in which the ZV-2 epitope was masked by introduction of a non-natural N-linked glycosylation site at position 375 in the ABDE sheet (M375N/ E377T double mutant) was found to exhibit improved neutralizing titers relative to ZDIII-WT in mice (Tai et al., 2019). Notwithstanding these observations, a recent study has suggested that EDIII-based immunogens might be less successful in primates, and that the CC' loop region is immunodominant (Yang et al., 2021).While we did not observe significant differences in protection between AaLS-ZDIII-WT and AaLS-rsZDIII-2.39 groups, it is possible that alternative dosing and adjuvant schemes might reveal differences. Nonetheless, the fact that AaLS-rsZDIII-2.39 is resurfaced in both the ABDE sheet and CC' loop epitopes suggests that it is a potential candidate for testing in non-human primates.

Author Manuscript Author Manuscript Author Manuscript Author Manuscript

The potential to induce ADE between ZIKV and DENV remains a concern for vaccine design (Pierson and Graham, 2016; Thomas and Barrett, 2020). The AaLS-rsZDIII-2.39 immunogen reported here-in elicited ZIKV-specific neutralizing antibodies, similar to other EDIII designs, and showed a lower magnitude of induced ADE against DENV1 compared AaLS-ZDIII-WT. Most antibodies associated with ADE activity are directed toward cross-reactive epitopes on the fusion loop of EDII (Lai et al., 2008; Oliphant et al., 2007; Throsby et al., 2006), or the pr(M) protein that chaperones E during viral assembly, but is then released (albeit incompletely) during viral maturation and egress (Smith et al., 2016). While much of the fusion loop is buried in the three-dimensional structure of the pre-fusion E dimer, it is likely exposed to some degree on viral particles due to dynamic breathing motions (Kuhn et al., 2015). Recent reports have described subunit vaccines consisting of stabilized, dimeric ZIKV and DENV E ectodomain (sE), in which the pre-fusion conformation was enforced by inter-subunit disulfide bonds (Kudlacek et al., 2021; Slon-Campos et al., 2019).This construct effectively masked the fusion loop, and does not contain pr(M) protein, and thus elicits neutralizing but not infection enhancing antibody responses. An alternative approach, we minimized the antigenic surface to avoid cross-reactive ZIKV/DENV epitopes.

The concept of shaping antibody signatures by structurally-designed immunogens is gaining interest in vaccinology. Modifications to viral glycoproteins can improve structural homogeneity, stabilize relevant oligomerization states, remove or mask highly variable regions, or fine-tune epitopes as we have done here. One attractive feature to structurally-designed immunogens is that they can be rapidly converted to mRNA or other vectored vaccine delivery platforms as was done with the SARS-CoV-2- stabilized spike ectodomain (Corbett et al., 2020; Jackson et al., 2020). The results reported here provide further evidence that antibody response can be altered by subtle variations in sequence design as well as antigen display. Ultimately, such strategies could be applied to target a wide range of viral pathogens.

SIGNIFICANCE

ZIKV and DENV are arthropod-borne pathogens which affect millions of people annually, yet have no approved anti-viral treatments. The development of vaccines has proven challenging, and is complicated by ADE, which can exacerbate subsequent infection if immunogens elicit cross-reactive but poorly neutralizing antibodies.

In this work, we utilized structure-guided protein design and phage display to engineer resurfaced rsZDIII immunogens where the LR epitope, which is engaged by protective antibodies, is maintained but regions of the ABDE sheet and CC’ loop, which are bound by non- or variably-neutralizing antibodies, were masked by mutations leading to amino acid substitution. One resurfaced nanoparticle immunogen (AaLS-rsZDIII-2.39) elicited a robust protective immune response in mice, but with significantly reduced numbers of ZIKV EDIII-reactive B cells and a lower magnitude of detected serum ADE against DENV1, relative to ZDIII-WT immunized animals, suggesting an immune focused response.

Author Manuscript Author Manuscript Author Manuscript Author Manuscript

Our results provide further evidence that antibody responses can be greatly affected by subtle variations in protein-antigen sequence and presentation, and holds the promise that flavivirus EDIII immunogens may potentially be further developed into viable vaccine candidates.

STAR METHODS TEXT

RESOURCE AVAILABILITY

Lead contact—Further information and requests for resources and reagents should be directed to and will be fulfilled by the Lead Contact Jonathan R. Lai (jon.lai@einsteinmed.edu).

Materials Availability—All requests for resources and reagents should be directed to the Lead Contact author. This includes mice and viruses. All reagents will be made available on request after completion of a Materials Transfer Agreement.

Data and Code Availability

- **Data.** All serological results described in this study are available within the body of the paper. All data (including raw data used to generate neutralizing and binding curves) reported in this paper will be shared by the lead contact upon request.
- **Code.** This paper does not report original code.
- **Additional information.** Any additional information required to reanalyze the data reported in this paper is available from the lead contact upon request.

EXPERIMENTAL MODEL AND SUBJECT DETAILS

Mouse immunization experiments were carried out at the Albert Einstein College of Medicine in accordance with the Guide for the Care and Use of Laboratory Animals of the National Institutes of Health after approval by the Institutional Animal Care and Use Committee. Female BALB/C mice (aged 6- to 8- weeks) were obtained from Charles River Laboratories and housed in vented cages with ad libitum diet.

All ZIKV lethal challenge studies were carried out in accordance with the recommendations in the Guide for the Care and Use of Laboratory Animals of the National Institutes of Health, and the protocols were approved by the Institutional Animal Care and Use Committee at the Washington University School of Medicine (assurance no. A3381–01). Male C57BL/6J mice (aged 9- to 10-weeks) were obtained from the Jackson Laboratory and housed in vented cages with ad libitum diet. To minimize animal suffering, injections were performed under anesthesia using a cocktail of ketamine hydrochloride and xylazine.

METHOD DETAILS

Phage display, library production and selection—An *E. coli*-optimized sequence encoding ZDIII-WT (H/PF/2013 strain, residues G302-K409, Table S1.) was cloned into phagemid pHP153 as previously described (Frei et al., 2015; Frei and Lai, 2016) for

Author Manuscript Author Manuscript Author Manuscript Author Manuscript

bivalent display of ZIKV EDIII, as a fusion to the minor coat protein pIII. Briefly, the pHP153 vector was first prepared by overnight digestion with NsiI and FseI restriction enzymes, and then isolated by gel extraction and DNA purification. The *E. coli*-optimized gene fragments encoding ZDIII-WT were then cloned into the digested vector using Gibson assembly (NEB), as per manufacturer's instructions. The construct included an N-terminal FLAG tag (DYKDDDDK) for detection. Resurfacing libraries were generated via oligonucleotide-based Kunkel mutagenesis, where positions targeted for randomization were varied according to the alanine scanning restricted diversity degenerate codons described elsewhere(Weiss et al., 2000). Briefly, uracil enriched single stranded DNA template (dU-ssDNA) was first isolated from phage propagated in a CJ236 strain of *E. coli,* which lacks dUTPase and uracil-N-glycosylate activity (*dut*⁻, *ung*⁻). We produced phage in the CJ236 strain in 2xYT media containing 0.25 μg/mL uridine, resulting in high levels of uracil incorporation into the phage genome.

dU-ssDNA template (10 μg) was incubated with a 3-fold molar excess of 5' phosphorylated mutagenesis library primers (Key Reagents Table) using a touchdown temperature annealing protocol of − 1°C/min from 95°C to 20°C (Frei and Lai, 2016; Huang et al., 2012). We added 20 U T7 DNA polymerase, 2 U T4 DNA ligase, and 940 μM dNTPs to the mixture, and the reaction was incubated at room temperature (RT) for 3 h, resulting in formation of cccDNA. Library DNA was purified using PCR reaction clean-up columns (Qiagen), with elution in 50 μL of sterile water. The library DNA was then electroporated into SS320 *E. coli* cells and infected with ~10^{10} PFU/ mL M13KO7 helper phage for 1 h at 37°C with shaking at 220 RPM. The rescue culture was transferred to flasks containing 1 L 2xYT/ 50 μg kanamycin/ 50 μg carbenicillin and allowed to grow overnight at 37°C, shaking at 220 RPM. The *E. coli* cultures were centrifuged at 3,000 g for 15 min to pellet and remove bacterial cells. The phage library in the supernatant was precipitated with 4% polyethylene glycol (PEG)-8000 (w/v) and 3% NaCl (w/v) by incubating on ice for 30 min, followed by centrifugation at 17,000 g for 20 min at 4°C. Phage pellets were resuspended in 1mL of PB-T (phosphate buffered saline (PBS) pH 7.4, 0.5% BSA (w/v), and 0.5% Tween-20 (v/v)), and the phage titer of the library was subsequently determined. Sterile glycerol was added to the library to a concentration of 50% (v/v), after which the library phage was flash frozen in liquid nitrogen (LN_2) and stored at −80°C.

To isolate resurfaced ZIKV EDIII mutants which retained binding to mAb ZV-67 with reduced binding to mAbs ZV-64 and ZV-2, the alanine phage library was subjected to two rounds of selection. The first round included positive selection against mAb ZV-67, whereas the second round of selection included negative selection against mAbs ZV-64 and ZV-2 followed by positive selection against mAb ZV-67 prior to phage amplification. For each selection, wells were coated with 0.5 μg per well of mAbs ZV-67, ZV-64, or ZV-2 and blocked with 1% BSA (w/v) in PBS for 2 h at RT. A well containing 1% BSA (w/v) in PBS served as the negative control in each round of selection. Phage were added and incubated for 1 h at room temperature (RT). For positive selections, unbound phage were removed by washing with PBS-T (PBS pH 7.4, 0.5% Tween-20 (v/v)). For negative selections, unbound phage were collected and incubated with the next target antibody for 1 h at RT. Following each positive selection, bound phage were eluted with 100 mM glycine pH 2.0 and collected into 2 M Tris-HCl pH 7.5. The output phage populations were amplified by infecting *E.*

Author Manuscript Author Manuscript Author Manuscript Author Manuscript

coli XL1-Blue cells and co-infecting with M13KO7 helper phage. Subsequently, phage were harvested by precipitation out of culture supernatant with 4% PEG-8000 (w/v) and 3% NaCl (v/v) and centrifugation at 17,000 g for 20 min at 4°C before resuspension in PB-T, as described previously(Frei and Lai, 2016; Frei et al., 2018).

Following selections, individual phage clones were screened by monoclonal phage ELISA as previously described (Frei and Lai, 2016; Frei et al., 2018). Briefly, individual phage clones were grown in a 96-deep well plate in 1-ml cultures with 2xYT medium supplemented with 100 μg/mL carbenicillin and 10^{10} IU/ml of helper phage. The monoclonal phage-containing supernatant was collected following removal of cells by centrifugation. Plates coated with mAbs ZV-67, ZV-64, and ZV-2 (0.5 μg per well) or anti-FLAG mAb M2 (Sigma) in PBS pH 8.0 overnight at 4°C were blocked for 2 h at RT with 1% BSA (w/v) in PBS. Phage-containing supernatant was added and incubated for 1 h at RT. Wells were washed with PBS-T, followed by addition of horseradish peroxidase (HRP)-conjugated anti-M13 mAb (1:1000 dilution) in PB-T for 1 h at RT. Wells were washed as before. The ELISA was developed with 3,3',5,5'-tetramethylbenxidine (TMB, Sigma) and quenched with 0.5 M H_2SO_4, after which absorbance at 450 nm was measured using a Synergy4 plate reader (Biotek). Clones that exhibited a >2 fold preference for binding to mAb ZV-67 over mAbs ZV-64, ZV-2, and BSA, were chosen for further characterization by full curve phage ELISA.

Mammalian Tissue Culture

Vero cells were grown in T300 flasks in DMEM high glucose media (Hyclone), supplemented with 10% fetal bovine serum (FBS, v/v, Hyclone), 1% penicillin/streptomycin (v/v), 20 mM L-glutamine at 37°C, 5% CO_2. Cell passaging was done by trypsinization, followed by quenching of enzyme activity by addition of an equal volume of supplemented medium. Cell passage numbers were tracked and did not exceed 30.

ExpiCHO cells (ThermoFisher) were grown and passaged according to the manufacturer's protocol in ExpiCHO serum free media (ThermoFisher) using 25 mL non-baffled flasks, at 37°C, 8% CO_2, and 120 RPM shaking.

Expression and Purification of ZDIII-WT and rsZDIIIs

Synthetic gene sequences encoding ZDIII-WT and rsZDIII sequences, including a C-terminal SpyTag (AHIVMVDAYKPTK), were codon optimized for expression in *E.coli* and obtained from a commercial supplier (Genewiz). The fragments were cloned into a pET-His6 MBP TEV cloning vector using Gibson assembly. Using this expression vector, rsZDIIIs were produced as a C-terminal fusion to maltose binding protein (MBP). A hexahistidine (His6) tag at the N-term of the MBP enabled downstream purification by nickel nitrilotriacetic acid (Ni-NTA) chromatography. Plasmids were transformed into BL21 Star chemically competent *E. coli* (ThermoFisher), and a single colony was used to inoculate a 5 mL 2xYT/ 50 μg/mL kanamycin culture for overnight growth at 37°C and 220 RPM. The starter culture was used to inoculate 0.5 L 2xYT cultures supplemented with 50 μg/mL of kanamycin, which were grown at 37°C and 220 RPM to an OD_{600} = 0.6 and thereafter induced by the addition of 0.8 μM isopropyl-β-D-1-thiogalactopyranoside (IPTG)

Author Manuscript Author Manuscript Author Manuscript Author Manuscript

and allowed to grow for 3 h at 28°C with shaking 220 RPM. Bacteria were pelleted by centrifugation 3,000 g for 15 min at 4°C, then frozen at −20°C.

Following a freeze-thaw cycle, the bacterial pellet was re-suspended in 40 mL of native solubility buffer (50 mM Tris-HCl pH 8.0, 250 mM NaCl, and 10 mM Imidazole) containing 3 U/mL Benzonase endonuclease (EMD-Millipore). Three sonication cycles of 30 s bursts were used to lyse cells using a sonicator (Fisher Scientific), after which the bacterial lysate was clarified to remove insoluble material by centrifugation at 17,000 g for 30 min at 4°C. Clarified lysate was added to Ni-NTA resin (Goldbio) and allowed to bind for 2 h at 4°C. The resin was washed extensively with wash buffer (50 mM Tris-HCl pH 8.0, 250 mM NaCl, and 20 mM Imidazole), and bound proteins were eluted with 50 mM Tris-HCl pH 8.0, 250 mM NaCl, and 250 mM Imidazole). The eluent was filtered using a 0.22 μm syringe filter (Millipore) and a His6-TEV protease was added at a 1:50 mg ratio. The mixture was transferred into 3,500 MWCO dialysis tubing (ThermoScientific) and dialyzed overnight at 4°C into buffer containing 50 mM Tris-HCl pH 9.0, and 20 mM NaCl.

Following dialysis, the protein mixture was again filtered to remove insoluble proteins, and loaded onto a MonoQ 10/300GL anion exchange column mounted on an AKTA pure FPLC platform (GE Healthcare). A linear salt gradient buffer (50 mM Tris-HCl pH 9.0 and 1 M NaCl) was used to elute bound proteins. Fractions were analyzed by SDS-PAGE gel and coomassie staining, then pooled and incubated with 0.7 mL of Ni-NTA resin for 90 min. This step removed remaining contamination of TEV, MBP, and uncut MBP-rsZDIII fusion proteins. Purified rsZDIIIs were buffer exchanged into storage buffer (20 mM Tris-HCl pH 8.0, 150 mM NaCl) and concentrated to 1 mg/mL using a 3,500 MWCO centrifugal filter (Millipore).

Soluble rsZDIIIs ELISA

Binding profiles of ZIKV mAbs (ZV-2, ZV-64, and ZV-67) to soluble rsZDIIIs were determined by ELISA. Briefly, half-area high-binding plates (Corning) were coated with 0.2 μg/ well of rsZDIIIs in PBS pH 8.0 and incubated overnight at 4°C. The next day, plates were blocked by incubation with PBS pH 7.4 containing 1% BSA (w/v) for 1.5 h with shaking, followed extensive washing with PBS pH 7.4 containing 0.05% Tween-20 (v/v). The mAbs were serially diluted in PB-T and then allowed to bind for 1 h with shaking at RT. After additional washing, a 1:2,000 dilution of protein A-HRP (ThermoFisher) was added to the plates and allowed to bind for 1 h. Plates were washed, and then TMB was added to each well. The reaction was allowed to proceed for 2.5 min after which it was quenched by addition of an equal volume of 0.5 M H_2SO_4. Absorbance at 450 nm was measured using a Synergy4 plate reader (Biotek) and data were fit to a four-parameter logistic regression equation using GraphPad Prism 8 to obtain EC_{50} values.

Biolayer inferometry (BLI)

BLI on an OctetRed system (ForteBio, Pall LLC) was used to measure the binding affinity of ZIKV antibodies to rsZDIII-2.39. Briefly, His6-MBP-rsZDIII-2.39 fusion proteins were serially diluted to different concentrations (188 nM, 94 nM, 47 nM, or 24 nM) then immobilized on Ni-NTA biosensors (Pall Life sciences). Association and dissociation

Author Manuscript Author Manuscript Author Manuscript Author Manuscript

kinetics were measured for interactions with 8 nM solutions of mAbs ZV-2, ZV-64, and ZV-67. A global 1:1 binding model was then used to estimate values for the association rate constant (k_{on}), the dissociation rate constant (k_{off}), and the apparent equilibrium dissociation constant (Kd^{app}) for each interaction. An MBP-alone negative control was used, which showed no binding to the mAbs tested (Supplemental Figure 3B).

Structural Analysis of rsZDIII-2.39 by NMR

To assess and compare the core structure of resurfaced rsZDIII-2.39 to ZDIII-WT, we prepared a [^{15}N]-rsZDIII-2.39 in M9 minimal media and acquired 2D NMR spectra. Using the pET-His6 MBP TEV cloning vector described above, we expressed rsZDIII-2.39 as a MBP-fusion protein in *E. coli* BL21 Star. Briefly, a starter culture was used to inoculate flasks containing 0.5 L M9 minimal media (6.5 g/L sodium phosphate dibasic, 3 g/L potassium phosphate monobasic, 0.5 g/L NaCl) supplemented with 50 μg/mL kanamycin, 2 g/L D-glucose, 1 mM MgSO4, 1× Trace Metal Mix A5, 1× MEM Vitamin Solution, and 1 g/L $^{15}NH_4Cl$. Cultures were grown at 37°C and 220 RPM to a density of OD_{600} = 0.6 and thereafter induced by the addition of 0.8 μM IPTG for 3 h at 28°C with shaking 220 RPM. Bacteria were then pelleted by centrifugation at 3,000 × g for 15 min at 4°C, and then frozen at −20°C. Purification of the [^{15}N]-rsZDIII-2.39 was done by Ni-NTA and anion exchange chromatography as described above in detail.

We collected NMR data at 300°K on a Bruker AVIII 600MHz spectrometer equipped with a 5 mm H&F TCI cryoprobe with z-axis gradients. The sample consisted of ~400 uM [15N]-rsZDIII-2.39 in 20 mM phosphate pH 6.0, 50 mM NaCl with TSP in 90% H_2O/ 10% D_2O in a 3 mm NMR tube. Data were processed in either Bruker Topspin or NMRPIPE software (Delaglio, 1995) and analysis was carried out in CcpNMR analysis software (Vranken et al., 2005). Backbone assignment of the 2.39 construct involved collecting 2D 1H-15N HSQC, 3D HNHA, 3D 15N NOESY-HSQC with 120 ms mixing time and 3D 15N TOCSY-HSQC with 60 ms mixing time and comparing chemical shifts against the wild-type construct shifts deposited in BMRB as 34167 (Wang et al., 2017). Many amide shifts in the 2.39 construct were assigned on the basis of overlapping with or being close to the WT HN, N, and Hα shifts. HSQC cross peaks of 2.39 that were not a close match were assigned on the basis of connections made via the 3D 15N NOESY-HSQC and 3D 15N TOCSY-HSQC spectra. Chemical shift differences between HSQC cross peaks for the WT and 2.39 spectra were calculated using the following equation, where $\Delta\delta_{HN}$ is the difference in chemical shift in the proton dimension, ΔδN is the difference in chemical shift in the nitrogen dimension, and αN is a scaling factor of 0.2:

$$CSP = \sqrt{(\Delta\delta_{NH})^2 + (\Delta\delta_N \times \alpha_N)^2}$$

AaLS nanoparticle Expression and rsZDIII Coupling—*Aquifex aeolicus* Lumazine synthase sequences were engineered to include a C-terminal SpyCatcher moiety (Supplement Table 1) and an N-terminal His6 tag, then codon optimized for expression in *E. coli* and ordered as synthetic gene fragments (Genewiz). The fragments were cloned into a pET28a expression vector (Sigma Aldrich) using Gibson assembly (NEB). The plasmid was

Author Manuscript Author Manuscript Author Manuscript Author Manuscript

then transformed into BL21 Star chemically competent *E. coli* cells (ThermoFisher), and a single colony was used to inoculate a 5mL 2xYT starter culture with 50 μg/mL kanamycin This culture was used to inoculate four 0.5 L 2xYT cultures, which were grown at 37°C and 220 RPM to an OD_{600} = 0.6 and thereafter induced by the addition of 0.2 μM isopropyl-β-D-1-thiogalactopyranoside (IPTG) for overnight at 22°C with shaking 220 RPM. Bacteria were pelleted by centrifugation at 3,000 g for 15 min at 4°C, and then frozen at −20°C. Ni-NTA purification was carried out, as is described above for the rsZDIII proteins, and the eluent containing AaLS-SpC nanoparticles was transferred into 10,000 MWCO dialysis tubing (ThermoScientific) and dialyzed overnight into a 50 mM Tris-HCl pH 8.0, 150 mM NaCl buffer. Recovered protein was loaded on a S400 gel filtration column to purify a homogeneous population of AaLS-SpC nanoparticles. Nanoparticles were concentrated to 1 mg/mL using a 10,000 MWCO centrifugal filter (Millipore), then filtered and flash frozen in LN_2 for storage at −80°C. Expressed AaLS-SpC nanoparticle preparations were analyzed by SDS-PAGE and coomassie staining.

In coupling reactions, a 3:1 molecular excess of rsZDIII-SpyTag was added to AaLS-SpyCatcher nanoparticles and allowed to gently mix on a rocker overnight (16 h) at RT. The reaction was filtered, then loaded on a S400 gel filtration column mounted on an AKTA pure FPLC platform to separate the coupled AaLS-rsZDIII nanoparticles from excess monomeric rsZDIII. Coupled AaLS-rsZDIII nanoparticles were concentrated to 1 mg/mL using a 10,000 MWCO centrifugal filter, then filtered and flash frozen in LN2 for storage at −80 °C.

Negative stain electron microscopy—400 mesh, carbon only grids were cleaned using a Tergeo-EM Plasma Cleaner (PIE Scientific, USA). Purified AaLS-rsZDIII-2.39 nanoparticles were adsorbed onto grids for 10 min, following washing with dH_2O. Samples were negatively stained with 1% uranyl acetate and viewed on a Tecnai 20 transmission electron microscope (ThermoFisher) at 120 kV.

Mouse immunizations—Groups of 6- to 8- week-old female BALB/c mice were immunized by 0.2 mL intraperitoneal injection using a 1 mL insulin syringe (BD). The vaccination schedule included a prime followed by two booster injections spaced 21 days apart. Addavax adjuvant was used in all immunizations, following the manufacturer's instructions for preparation. Mice received 15 μg of AaLS-rsZDIII nanoparticles or a 5 μg molar-adjusted dose of monomeric rsZDIII. Blood was collected from the animals by mandibular bleeds, one day prior to prime immunization and two weeks following each boost injection. Using a 5 mm lancet, the vascular bundle at the back of the jaw was punctured and up to 0.2 mL of blood was collected in a SST tube (BD) (Golde et al., 2005). Samples were allowed to coagulate at RT for 30–60 min then centrifuged for 2 min at 10,000 g to separate the serum. Serum was aliquoted and flash frozen in LN_2 for storage at −20°C.

Monoclonal antibody production—Publicly available sequences for the heavy and light chain variable regions of antibodies ZV-2, ZV-64, ZV-67, and E60 (Oliphant et al., 2006; Zhao et al., 2016) were ordered as gene fragments (Genewiz) and cloned into pMAZ mammalian expression vectors by Gibson assembly. Ten micrograms of each heavy and light chain DNA plasmids were co-transfected into ExpiCHO cells following the

Author Manuscript Author Manuscript Author Manuscript Author Manuscript

manufacturer's standard titer expression protocol, and cultures were allowed to grow 7–10 days at 37°C and 120 RPM. The supernatant was then harvested by centrifugation at 3,000 g for 20 min at 4°C, and filtered using a 0.22μm syringe filter (Millipore). Antibodies were purified using protein A agarose resin (Goldbio) and the Gentle Antibody Elution system (ThermoScientific Pierce) following the manufacturer's protocol. Purified antibodies were desalted using PD-10 columns (GE healthcare) into a 150 mM HEPES pH 7.4 buffer containing 200 mM NaCl, then quantified by UV-spectrometry measurement at 280 nm and flash frozen in LN_2 for storage at −20°C.

Serum ELISA—Half-area high binding plates (Corning) were coated with 0.2 μg/well of rsZDIIIs in PBS pH 8.0 overnight at 4°C. Coated plates were blocked for 90 min with 1% BSA at RT, then extensively washed using PBS-T buffer (PBS pH 7.4, 0.05% Tween-20 (v/v). Serum was serially diluted in PB-T buffer (PBS pH 7.4, 1% BSA (w/v), 0.05% Tween-20 (v/v), added to plates and incubated for 60 min at RT with shaking. Following additional washing, a 1:2,000 dilution of goat anti-mouse HRP antibody was added to the plates for 60 min at RT. Following washing with PBS-T, plates were developed by addition of 50 μL of TMB at RT for 2.5 min, then quenched with 50 μL of 0.5 M H_2SO_4. Binding was measured by detection of OD_{450} on a Synergy4 plate reader (Biotek). EC_{50} values were determined by fitting a four parameter logistics curve using GraphPad Prism 8.

Virus propagation—ZIKV (H/PF/2013 stain) was propagated by confluent Vero cells at an MOI of 0.05–0.01. Plates were incubated at 37°C for up to 72 h or until cytopathic effects were observed. Supernatant from the plates was collected and sterile filtered using a 0.45 μm syringe filter (Millipore), and then aliquoted and flash frozen in LN_2 and stored at −80°C.

Reporter virus particle (RVP) production—Reporter virus particles (RVPs) incorporating the structural proteins of DENV1 (strain West Pac-74), DENV2 (strain New Guinea C), or DENV4 (strain 814669) were produced by complementation of a subgenomic GFP-expressing replicon derived from a lineage II strain of WNV as previously described (Burgomaster et al., 2021; VanBlargan et al., 2015). Briefly, HEK-293T cells were transfected with plasmids encoding the replicon and structural genes at a 1:3 ratio by mass using Lipofectamine 300 (Invitrogen), followed by incubation at 30°C. RVP-containing supernatant was harvested from cells at days 3–6 post-transfection, filtered through a 0.22 μm filter, and stored at −80°C. To determine virus titer, two-fold dilutions of RVPs were used to infect Raji cells that express the flavivirus attachment factor DC-SIGNR in duplicate technical replicates at 37°C. GFP-positive infected cells were detected by flow cytometry 2 days later. In subsequent ADE assays, RVPs were sufficiently diluted to within the linear range of the virus-infectivity dose-response curve to ensure antibody excess at informative points.

Antibody-dependent enhancement (ADE) assay—RVPs were mixed with serial dilutions of heat-inactivated mouse sera or monoclonal antibodies for 1 h at 37°C, followed by infection of K562 erythroleukemic cells that express the Fcγ receptor IIA (CD32A) in duplicate technical replicates. Infections were carried out at 37°C and GFP-positive infected cells quantified by flow cytometry 2 days later. Type-specific neutralizing E

Author Manuscript Author Manuscript Author Manuscript Author Manuscript

DIII-reactive mAbs were run in parallel for each RVP and used for normalization (peak infectivity of type-specific mAb = 100). All control mAbs were isotype IgG2c: DENV1 (mAb DV1-E106), DENV2 (mAb DV2–96), DENV4 (mAb DV4-E88) (Shrestha et al., 2010; Sukupolvi-Petty et al., 2010; Sukupolvi-Petty et al., 2013).

Focus reduction neutralization test (FRNT)—The neutralizing capacity of the serum was characterized by FRNT, which has been previously described (Zhao et al., 2016). Briefly, the collected serum was serially diluted in DMEM media containing 2% (v/v) FBS (HyClone) and incubated with ~100 FFU ZIKV (H/PF/2013 strain) for 60 min at 37 °C, 5% CO_2. Triplicates of each dilution were added to 96 well tissue culture plates (Corning) seeded with a monolayer of Vero cells, and incubated for 60 min at 37°C, 5% CO_2. A 150 μL overlay (carboxymethylcellulose, 1× MEM, 2% FBS (v/v), and 10 mM HEPES) was added to each well, and infection was allowed to proceed 40 h. Plates were then fixed with 1% paraformaldehyde in PBS pH 7.4 for 60 min at RT, washed using PBS pH 7.4, then permeabilized in permeabilization/wash buffer (PBS pH 7.4, 0.1% saponin (w/v), 0.1% BSA (w/v). An anti-flavivirus fusion loop mAb E60 (Oliphant et al., 2006) was added at 1 μg/mL in permeabilization/ wash buffer, then plates were incubated overnight at 4°C. Plates were thoroughly washed in PBS pH 7.4, then protein A-HRP (Invitrogen) was added at 1:2000 for 60 min. Following washing, 50 μL TrueBlue reagent (Seracare) were added and the plates were allowed to develop up to 30 min. Plates were imaged and foci quantitated on a BioSpot reader (Immunospot). The data were analyzed by fitting a four parameter logistics curve (GraphPad Prism) to determine reported $FRNT_{50}$ values.

ZIKV lethal challenge studies—Blood was collected from AaLS-rsZDIII-2.39 and AaLS-ZDIII immunized animals on day 56 via cardiac puncture following euthanasia. Samples were allowed to coagulate in a SST tube at RT for 30–60 min, then centrifuged for 2 min at 10,000 g to separate the serum. Collected sera from each group were then pooled to provide sufficient material for passive transfer studies in 9- to 10-week-old C57BL/6J male mice (Jackson Laboratory).The ZIKV viral challenge model used herein is extensively described elsewhere (Gorman et al., 2018). Briefly, one day prior to ZIKV challenge, mice were injected via i.p. route with 2 mg of an anti-Ifnar1 mAb (clone MAR1–5A3) and 100 μL of naïve control or pooled day 56 serum. The following day, mice were inoculated by subcutaneous injection in the footpad with 3×10^5 FFU of ZIKV (strain Dakar 41525). Mice were subsequently monitored for survival and changes in weight for 21 days, at which point surviving mice were euthanized.

Splenocyte isolation and antigen-reactive B cell analysis by flow cytometry —Spleens were isolated from vaccinated animals at day 56, and single-cell splenocyte suspensions were prepared by mechanical tissue dissociation. Briefly, spleens were gently minced using sterile scissors, then passed through a 70 μm cell strainer using a 3mL syringe plunger; sterile PBS buffer containing 2% FBS (v/v) was used to dislodge and flush freed single-cells from the strainer. A brief hypotonic lysis using 0.2% (w/v) NaCl to remove red blood cells, followed by adjustment of salinity to isotonic conditions. Cells were cryopreserved in FBS containing 10% dimethyl sulfoxide (DMSO, v/v) and stored at −80 °C until analysis. The ZDIII-WT FACS-probe was expressed in *E. coli* and

Author Manuscript Author Manuscript Author Manuscript Author Manuscript

purified as described above, after which the molecule was biotinylated using an EZ-Link™ NHS-PEG4-Biotinylation kit (ThermoFisher) according to manufacturer's instructions. Splenocytes were stained with 200 nM ZDIII-WT FACS-probe and anti-CD3, CD8a, F4/80, Gr-1, CD-19, IgG antibodies (see Key Reagents Table) at a 1:100 dilution, followed by secondary staining with Strepavidin-PE (1:500 dilution). Splenocytes were filtered through a 70 μm cell strainer and 1×10^6 events were acquired and analyzed on a LSRII analyzer (BD) following the gating strategy shown (Figure S6).

Quantification and Statistical Analysis—Analysis of data was done using GraphPad Prism8 software according to statistical methods indicated. FRNT neutralization and cross-reactivity data was analyzed by 2-way ANOVA with Tukey's multiple comparisons test. Survival in ZIKV lethal challenge studies was analyzed using the log-rank Mantel-Cox test with a Bonferroni correction. Change in initial animal weight following ZIKV infection was analyzed by 2-way ANOVA with Sidak's post-test relative to the AaLS-control group. The frequency of antigen-reactive splenic B cells in flow cytometry experiments was analyzed by unpaired student's t-test. Values were considered significant at *p< 0.05, **p<0.01, ***p<0.001, ****p<0.0001.

Supplementary Material

Refer to Web version on PubMed Central for supplementary material.

ACKNOWLEDGMENTS

The NMR analysis made use of NMRbox: National Center for Biomolecular NMR Data Processing and Analysis, a Biomedical Technology Research Resource (BTRR), which is supported by NIH grant P41GM111135 (NIGMS). We gratefully acknowledge technical assistance from the Einstein Analytical Imaging Facility and the Einstein Flow Cytometry Core, which is in part supported by NIH grant P30CA013330. This work was supported by the National Institutes of Health (R01-AI158194 to J.R.L, R01 AI073755 to M.S.D., and intramural program of NIAID to T.C.P.). G.I.G. and A.S.W. were supported in part by NIH training grants (T32-GM99749 and T32-AI070117). R.J.M was supported in part by NIH training grants (T32GM007288 and F30AI150055). A.W.W. was supported by an NIH pre-doctoral training grant award (T32 5T32AI007172-38) and the Medical Scientist Training Program. E. K. N. was supported in part by a postdoctoral fellowship from the Deutscher Akade-mischer Austauschdienst (German Academic Exchange Service). The Bruker 600 MHz NMR instrument in the Structural NMR Resource at the Albert Einstein College of Medicine was purchased using funds from NIH award 1S10OD016305 and is supported by a Cancer Center Support Grant (P30 CA013330).

DECLARATION OF INTERESTS

A US Patent Application describing the rsZDIII clones has been submitted with J.R.L., G.I.G., A.S.W., and E.K.N. as co-inventors. J.R.L. is a consultant for Celdara Medical, LLC. .M.S.D. is a consultant for Inbios, Vir Biotechnology, Senda Biosciences, and Carnival Corporation and on the Scientific Advisory Boards of Moderna and Immunome. The Diamond laboratory has received unrelated funding support in sponsored research agreements from Moderna, Vir Biotechnology, and Emergent BioSolutions.

REFERENCES

Andrade P, Gimblet-Ochieng C, Modirian F, Collins M, Cardenas M, Katzelnick LC, Montoya M, Michlmayr D, Kuan G, Balmaseda A, et al. (2019). Impact of pre-existing dengue immunity on human antibody and memory B cell responses to Zika. Nat Commun 10, 938. [PubMed: 30808875]

Brasil P, Pereira JP Jr., Moreira ME, Ribeiro Nogueira RM, Damasceno L, Wakimoto M, Rabello RS, Valderramos SG, Halai UA, Salles TS, et al. (2016). Zika Virus Infection in Pregnant Women in Rio de Janeiro. N Engl J Med 375, 2321–2334. [PubMed: 26943629]

Author Manuscript Author Manuscript Author Manuscript Author Manuscript

Brouwer PJM, Antanasijevic A, Berndsen Z, Yasmeen A, Fiala B, Bijl TPL, Bontjer I, Bale JB, Sheffler W, Allen JD, et al. (2019). Enhancing and shaping the immunogenicity of native-like HIV-1 envelope trimers with a two-component protein nanoparticle. Nat Commun 10, 4272. [PubMed: 31537780]

Burgomaster KE, Foreman BM, Aleshnick MA, Larman BC, Gordon DN, Maciejewski S, Morabito KM, Ledgerwood JE, Gaudinski MR, Chen GL, et al. (2021). Limited Flavivirus Cross-Reactive Antibody Responses Elicited by a Zika Virus Deoxyribonucleic Acid Vaccine Candidate in Humans. J Infect Dis 224, 1550–1555. [PubMed: 33961055]

Cabral-Miranda G, Lim SM, Mohsen MO, Pobelov IV, Roesti ES, Heath MD, Skinner MA, Kramer MF, Martina BEE, and Bachmann MF (2019). Zika Virus-Derived E-DIII Protein Displayed on Immunologically Optimized VLPs Induces Neutralizing Antibodies without Causing Enhancement of Dengue Virus Infection. Vaccines (Basel) 7.

Cao-Lormeau V-M, Blake A, Mons S, Lastère S, Roche C, Vanhomwegen J, Dub T, Baudouin L, Teissier A, Larre P, et al. (2016). Guillain-Barré Syndrome outbreak associated with Zika virus infection in French Polynesia: a case-control study. The Lancet 387, 1531–1539.

Corbett KS, Edwards DK, Leist SR, Abiona OM, Boyoglu-Barnum S, Gillespie RA, Himansu S, Schafer A, Ziwawo CT, DiPiazza AT, et al. (2020). SARS-CoV-2 mRNA vaccine design enabled by prototype pathogen preparedness. Nature 586, 567–571. [PubMed: 32756549]

Dai L, Song J, Lu X, Deng YQ, Musyoki AM, Cheng H, Zhang Y, Yuan Y, Song H, Haywood J, et al. (2016). Structures of the Zika Virus Envelope Protein and Its Complex with a Flavivirus Broadly Protective Antibody. Cell Host Microbe 19, 696–704. [PubMed: 27158114]

Delaglio F, et al. (1995). NMRPipe: A multidimensional spectral processing system based on UNIX pipes* Journal of Biomolecular NMR 6, 277–293. [PubMed: 8520220]

Dick GW, Kitchen SF, and Haddow AJ (1952). Zika Virus Pathogenicity and Physical Properties. Transactions of the Royal Society of Tropical Medicine and Hygiene 46.

Duffy MR, Chen T, Hancock WT, Powers AM, Kool JL, Lanciotti RS, Pretrick M, Marfel M, Holzbauer S, Dubray C, et al. (2009). Zika Virus Outbreak on Yap Island, Federated States of Micronesia. The New England Journal of Medicine 360, 2536–2543. [PubMed: 19516034]

Frei JC, Kielian M, and Lai JR (2015). Comprehensive mapping of functional epitopes on dengue virus glycoprotein E DIII for binding to broadly neutralizing antibodies 4E11 and 4E5A by phage display. Virology 485, 371–382. [PubMed: 26339794]

Frei JC, and Lai JR (2016). Protein and Antibody Engineering by Phage Display. Methods Enzymol 580, 45–87. [PubMed: 27586328]

Frei JC, Wirchnianski AS, Govero J, Vergnolle O, Dowd KA, Pierson TC, Kielian M, Girvin ME, Diamond MS, and Lai JR (2018). Engineered Dengue Virus Domain III Proteins Elicit Cross-Neutralizing Antibody Responses in Mice. J Virol 92.

Golde WT, Gollobin P, and Rodriguez LL (2005). A rapid, simple, and humane method for submandibular bleeding of mice using a lancet. Lab animal 34, 39–43.

Gorman MJ, Caine EA, Zaitsev K, Begley MC, Weger-Lucarelli J, Uccellini MB, Tripathi S, Morrison J, Yount BL, Dinnon KH 3rd, et al. (2018). An Immunocompetent Mouse Model of Zika Virus Infection. Cell Host Microbe 23, 672–685 e676. [PubMed: 29746837]

Guzman MG, Alvarez M, and Halstead SB (2013). Secondary infection as a risk factor for dengue hemorrhagic fever/dengue shock syndrome: an historical perspective and role of antibody-dependent enhancement of infection. Arch Virol 158, 1445–1459. [PubMed: 23471635]

Halstead SB (2003). Neutralization and antibody-dependent enhancement of dengue viruses. Adv virus res 60, 421–467. [PubMed: 14689700]

Havenar-Daughton C, Carnathan DG, Boopathy AV, Upadhyay AA, Murrell B, Reiss SM, Enemuo CA, Gebru EH, Choe Y, Dhadvai P, et al. (2019). Rapid Germinal Center and Antibody Responses in Non-human Primates after a Single Nanoparticle Vaccine Immunization. Cell Rep 29, 1756–1766 e1758. [PubMed: 31722194]

Heinz F, and Stiasny K (2017). The Antigenic Structure of Zika Virus and Its Relation to Other Flaviviruses: Implications for Infection and Immunoprophylaxis. Microbiology and Molecular Biology Reviews 81, e00055–00016. [PubMed: 28179396]

Author Manuscript Author Manuscript Author Manuscript Author Manuscript

Huang R, Fang P, and Kay BK (2012). Improvements to the Kunkel mutagenesis protocol for constructing primary and secondary phage-display libraries. Methods 58, 10–17. [PubMed: 22959950]

Irvine DJ, and Read BJ (2020). Shaping humoral immunity to vaccines through antigen-displaying nanoparticles. Curr Opin Immunol 65, 1–6. [PubMed: 32200132]

Jackson LA, Anderson EJ, Rouphael NG, Roberts PC, Makhene M, Coler RN, McCullough MP, Chappell JD, Denison MR, Stevens LJ, et al. (2020). An mRNA Vaccine against SARS-CoV-2 - Preliminary Report. N Engl J Med 383, 1920–1931. [PubMed: 32663912]

Katzelnick LC, Bos S, and Harris E (2020a). Protective and enhancing interactions among dengue viruses 1–4 and Zika virus. Curr Opin Virol 43, 59–70. [PubMed: 32979816]

Katzelnick LC, Narvaez C, Arguello S, Mercado BL, Collado D, Ampie O, Elizondo D, Miranda T, Carillo FB, Mercado JC, et al. (2020b). Zika virus infection enhances future risk of severe dengue disease. Science 369, 1123–1128. [PubMed: 32855339]

Kringelum JV, Nielsen M, Padkjaer SB, and Lund O (2013). Structural analysis of B-cell epitopes in antibody:protein complexes. Mol Immunol 53, 24–34. [PubMed: 22784991]

Kudlacek ST, Metz S, Thiono D, Payne AM, Phan TT, Tian S, Forsberg LJ, Maguire J, Seim I, Zhang S, et al. (2021). Designed, highly expressing, thermostable dengue virus 2 envelope protein dimers elicit quaternary epitope antibodies. Science advances 7.

Kuhn RJ, Dowd KA, Beth Post C, and Pierson TC (2015). Shake, rattle, and roll: Impact of the dynamics of flavivirus particles on their interactions with the host. Virology 479–480, 508–517.

Ladenstein R, and Morgunova E (2020). Second career of a biosynthetic enzyme: Lumazine synthase as a virus-like nanoparticle in vaccine development. Biotechnol Rep (Amst) 27, e00494. [PubMed: 32714852]

Lai CY, Tsai WY, Lin SR, Kao CL, Hu HP, King CC, Wu HC, Chang GJ, and Wang WK (2008). Antibodies to envelope glycoprotein of dengue virus during the natural course of infection are predominantly cross-reactive and recognize epitopes containing highly conserved residues at the fusion loop of domain II. J Virol 82, 6631–6643. [PubMed: 18448542]

Lazear HM, and Diamond MS (2016). Zika Virus: New Clinical Syndromes and Its Emergence in the Western Hemisphere. J Virol 90, 4864–4875. [PubMed: 26962217]

Lazear HM, Govero J, Smith AM, Platt DJ, Fernandez E, Miner JJ, and Diamond MS (2016). A Mouse Model of Zika Virus Pathogenesis. Cell Host Microbe 19, 720–730. [PubMed: 27066744]

Lin HH, Yang SP, Tsai MJ, Lin GC, Wu HC, and Wu SC (2019). Dengue and Zika Virus Domain III-Flagellin Fusion and Glycan-Masking E Antigen for Prime-Boost Immunization. Theranostics 9, 4811–4826. [PubMed: 31367259]

Mlakar J, Korva M, Tul N, Popovic M, Poljsak-Prijatelj M, Mraz J, Kolenc M, Resman Rus K, Vesnaver Vipotnik T, Fabjan Vodusek V, et al. (2016). Zika Virus Associated with Microcephaly. N Engl J Med 374, 951–958. [PubMed: 26862926]

Moyer TJ, Zmolek AC, and Irvine DJ (2016). Beyond antigens and adjuvants: formulating future vaccines. J Clin Invest 126, 799–808. [PubMed: 26928033]

Mukherjee M, Dutta K, White MA, Cowburn D, and Fox RO (2006). NMR solution structure and backbone dynamics of domain III of the E protein of tick-borne Langat flavivirus suggests a potential site for molecular recognition. Protein Sci 15, 1342–1355. [PubMed: 16731969]

Nybakken GE, Oliphant T, Johnson S, Burke S, Diamond MS, and Fremont DH (2005). Structural basis of West Nile virus neutralization by a therapeutic antibody. Nature 437, 764–769. [PubMed: 16193056]

Oehler E, Watrin L, Larre P, Leparc-Goffart I, Lastère S, Valour F, Baudouin L, Mallet HP, Musso D, and Ghawche F (2013). Zika virus infection complicated by Guillain-Barré syndrome – case report, French Polynesia, December 2013. Eurosurveillance 19, 20720.

Oliphant T, Nybakken GE, Austin SK, Xu Q, Bramson J, Loeb M, Throsby M, Fremont DH, Pierson TC, and Diamond MS (2007). Induction of epitope-specific neutralizing antibodies against West Nile virus. J Virol 81, 11828–11839. [PubMed: 17715236]

Oliphant T, Nybakken GE, Engle M, Xu Q, Nelson CA, Sukupolvi-Petty S, Marri A, Lachmi BE, Olshevsky U, Fremont DH, et al. (2006). Antibody recognition and neutralization determinants

Author Manuscript Author Manuscript Author Manuscript Author Manuscript

on domains I and II of West Nile Virus envelope protein. J Virol 80, 12149–12159. [PubMed: 17035317]

Pierson TC, and Diamond MS (2018). The emergence of Zika virus and its new clinical syndromes. Nature 560, 573–581. [PubMed: 30158602]

Pierson TC, and Graham BS (2016). Zika Virus: Immunity and Vaccine Development. Cell 167, 625–631. [PubMed: 27693357]

Pierson TC, Xu Q, Nelson S, Oliphant T, Nybakken GE, Fremont DH, and Diamond MS (2007). The stoichiometry of antibody-mediated neutralization and enhancement of West Nile virus infection. Cell Host Microbe 1, 135–145. [PubMed: 18005691]

Rasmussen SA, Jamieson DJ, Honein MA, and Petersen LR (2016). Zika virus and birth defects—reviewing the evidence for causality. New England Journal of Medicine 374, 1981–1987. [PubMed: 27074377]

Robbiani DF, Bozzacco L, Keeffe JR, Khouri R, Olsen PC, Gazumyan A, Schaefer-Babajew D, Avila-Rios S, Nogueira L, Patel R, et al. (2017). Recurrent Potent Human Neutralizing Antibodies to Zika Virus in Brazil and Mexico. Cell 169, 597–609 e511. [PubMed: 28475892]

Rogers TF, Goodwin EC, Briney B, Sok D, Beutler N, Strubel A, Nedellec R, Le K, Brown ME, Burton DR, et al. (2017). Zika virus activates de novo and cross-reactive memory B cell responses in dengue-experienced donors. Science immunology 2.

Roth A, Mercier A, Lepers C, Hoy D, Duituturaga S, Benyon E, Guillaumot L, and Souarès Y (2014). Concurrent outbreaks of dengue, chikungunya and Zika virus infections – an unprecedented epidemic wave of mosquito-borne viruses in the Pacific 2012–2014. Eurosurveillance 19, 20929. [PubMed: 25345518]

Sapparapu G, Fernandez E, Kose N, Bin C, Fox JM, Bombardi RG, Zhao H, Nelson CA, Bryan AL, Barnes T, et al. (2016). Neutralizing human antibodies prevent Zika virus replication and fetal disease in mice. Nature 540, 443–447. [PubMed: 27819683]

Shrestha B, Brien JD, Sukupolvi-Petty S, Austin SK, Edeling MA, Kim T, O'Brien KM, Nelson CA, Johnson S, Fremont DH, et al. (2010). The development of therapeutic antibodies that neutralize homologous and heterologous genotypes of dengue virus type 1. PLoS Pathog 6, e1000823. [PubMed: 20369024]

Sirohi D, Chen Z, Sun L, Klose T, Pierson TC, Rossmann MG, and Kuhn RJ (2016). The 3.8 Å resolution cryo-EM structure of Zika virus. Science 352, 467–470. [PubMed: 27033547]

Slon-Campos JL, Dejnirattisai W, Jagger BW, Lopez-Camacho C, Wongwiwat W, Durnell LA, Winkler ES, Chen RE, Reyes-Sandoval A, Rey FA, et al. (2019). A protective Zika virus E-dimer-based subunit vaccine engineered to abrogate antibody-dependent enhancement of dengue infection. Nat Immunol 20, 1291–1298. [PubMed: 31477918]

Smith SA, Nivarthi UK, de Alwis R, Kose N, Sapparapu G, Bombardi R, Kahle KM, Pfaff JM, Lieberman S, Doranz BJ, et al. (2016). Dengue Virus prM-Specific Human Monoclonal Antibodies with Virus Replication-Enhancing Properties Recognize a Single Immunodominant Antigenic Site. J Virol 90, 780–789. [PubMed: 26512092]

Stettler K, Beltramello M, Espinosa DA, Graham V, Cassotta A, Bianchi S, Vanzetta F, Minola A, Jaconi S, Mele F, et al. (2016). Specificity, cross-reactivity, and function of antibodies elicited by Zika virus infection. Science (New York, NY) 353, 823–826. [PubMed: 27417494]

Sukupolvi-Petty S, Austin SK, Engle M, Brien JD, Dowd KA, Williams KL, Johnson S, Rico-Hesse R, Harris E, Pierson TC, et al. (2010). Structure and function analysis of therapeutic monoclonal antibodies against dengue virus type 2. J Virol 84, 9227–9239. [PubMed: 20592088]

Sukupolvi-Petty S, Brien JD, Austin SK, Shrestha B, Swayne S, Kahle K, Doranz BJ, Johnson S, Pierson TC, Fremont DH, et al. (2013). Functional analysis of antibodies against dengue virus type 4 reveals strain-dependent epitope exposure that impacts neutralization and protection. Journal of virology 87.

Sun F, Zhang WB, Mahdavi A, Arnold FH, and Tirrell DA (2014). Synthesis of bioactive protein hydrogels by genetically encoded SpyTag-SpyCatcher chemistry. Proc Natl Acad Sci U S A 111, 11269–11274. [PubMed: 25049400]

Tai W, Chen J, Zhao G, Geng Q, He L, Chen Y, Zhou Y, Li F, and Du L (2019). Rational Design of Zika Virus Subunit Vaccine with Enhanced Efficacy. J Virol 93.

Author Manuscript Author Manuscript Author Manuscript Author Manuscript

Thomas SJ, and Barrett A (2020). Zika vaccine pre-clinical and clinical data review with perspectives on the future development. Hum Vaccin Immunother 16, 2524–2536. [PubMed: 32702260]

Throsby M, Geuijen C, Goudsmit J, Bakker AQ, Korimbocus J, Kramer RA, Clijsters-van der Horst M, de Jong M, Jongeneelen M, Thijsse S, et al. (2006). Isolation and characterization of human monoclonal antibodies from individuals infected with West Nile Virus. J Virol 80, 6982–6992. [PubMed: 16809304]

Tokatlian T, Read BJ, Jones CA, Kulp DW, Menis S, Chang JYS, J.M., Kumari S, Allen JD, Dane EL, and Liguori A (2019). Innate immune recognition of glycans targets HIV nanoparticle immunogens to germinal centers. Science 363, 649–654. [PubMed: 30573546]

Ulrich EL, Akutsu H, Doreleijers JF, Harano Y, Ioannidis YE, Lin J, Livny M, Mading S, Maziuk D, Miller Z, et al. (2008). BioMagResBank. Nucleic Acids Res 36, D402–408. [PubMed: 17984079]

VanBlargan LA, Davis KA, Dowd KA, Akey DL, Smith JL, and Pierson TC (2015). Context-Dependent Cleavage of the Capsid Protein by the West Nile Virus Protease Modulates the Efficiency of Virus Assembly. J Virol 89, 8632–8642. [PubMed: 26063422]

Vranken WF, Boucher W, Stevens TJ, Fogh RH, Pajon A, Llinas M, Ulrich EL, Markley JL, Ionides J, and Laue ED (2005). The CCPN data model for NMR spectroscopy: development of a software pipeline. Proteins 59, 687–696. [PubMed: 15815974]

Wang J, Bardelli M, Espinosa DA, Pedotti M, Ng TS, Bianchi S, Simonelli L, Lim EXY, Foglierini M, Zatta F, et al. (2017). A Human Bi-specific Antibody against Zika Virus with High Therapeutic Potential. Cell 171, 229–241 e215. [PubMed: 28938115]

Wang X, Tai W, Zhang X, Zhou Y, Du L, and Shen C (2019). Effects of Adjuvants on the Immunogenicity and Efficacy of a Zika Virus Envelope Domain III Subunit Vaccine. Vaccines (Basel) 7.

Watterson D, Kobe B, and Young PR (2012). Residues in domain III of the dengue virus envelope glycoprotein involved in cell-surface glycosaminoglycan binding. J Gen Virol 93, 72–82. [PubMed: 21957126]

Weiss GA, Watanabe CK, Zhong A, Goddard A, and Sidhu SS (2000). Rapid mapping of protein functional epitopes by combinatorial alanine scanning. Proc Natl Acad Sci U S A 97, 8950–8954. [PubMed: 10908667]

Yang R, Liu Q, Pang W, Gao F, Liang H, Zhang W, Lin Y, Li M, Liu Z, Gao GF, et al. (2021). Two immunogenic recombinant protein vaccine candidates showed disparate protective efficacy against Zika virus infection in rhesus macaques. Vaccine 39, 915–925. [PubMed: 33451779]

Zakeri B, Fierer JO, Celik E, Chittock EC, Schwarz-Linek U, Moy VT, and Howarth M (2012). Peptide tag forming a rapid covalent bond to a protein, through engineering a bacterial adhesin. Proc Natl Acad Sci U S A 109, E690–697. [PubMed: 22366317]

Zhao H, Fernandez E, Dowd KA, Speer SD, Platt DJ, Gorman MJ, Govero J, Nelson CA, Pierson TC, Diamond MS, et al. (2016). Structural Basis of Zika Virus-Specific Antibody Protection. Cell 166, 1016–1027. [PubMed: 27475895]

Author Manuscript Author Manuscript Author Manuscript Author Manuscript

Highlights

- Resurfacing of antigens by mutagenesis can selectively change antibody reactivity
- Display of flavivirus EDIIIs as nanoparticle immunogens enhances immune response
- Resurfaced immunogen (rsZDIII-2.39) elicits protective, immune-focused responses
- rsZDIII-2.39 produces fewer EDIII-reactive B cells, and a lower degree of serum ADE

Author Manuscript
Author Manuscript
Author Manuscript
Author Manuscript

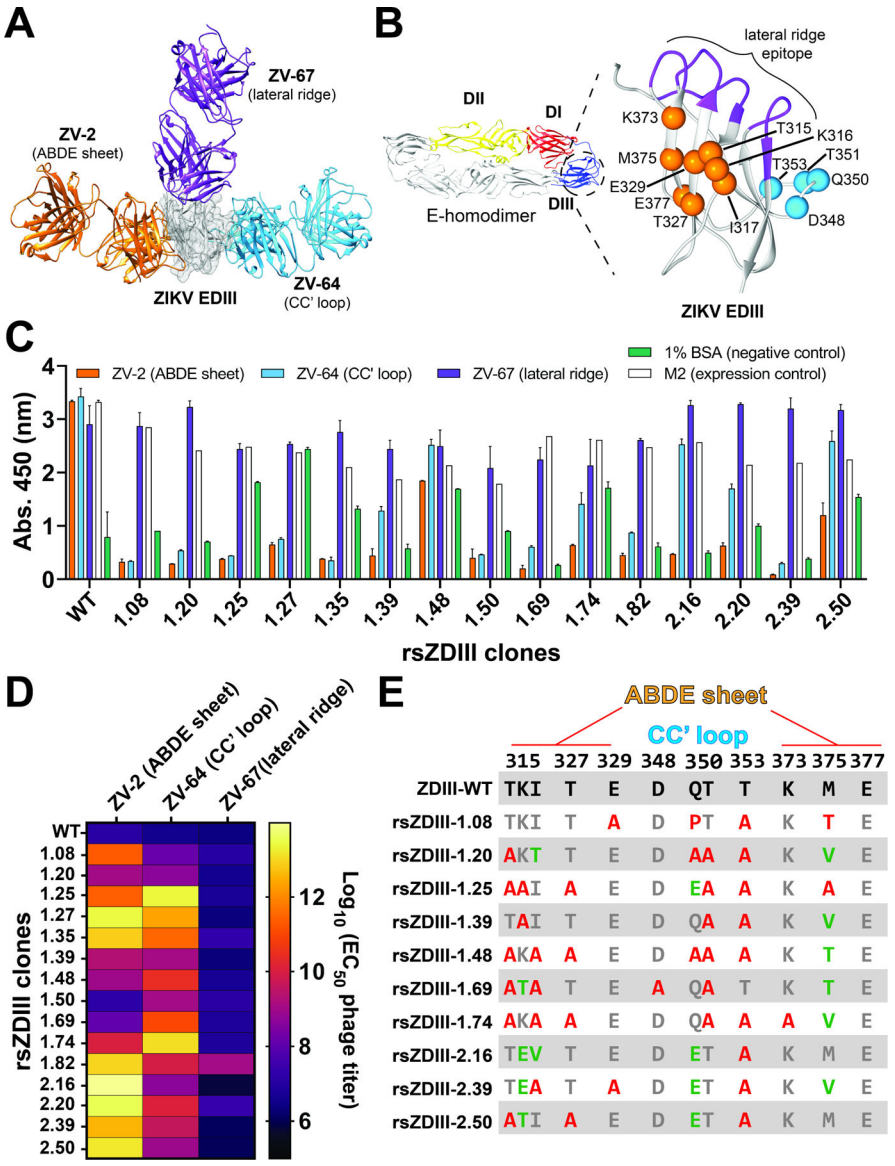

Figure 1. Isolation of resurfaced ZIKV-EDIII variants (rsZDIIIs) by phage display.

(A) Structural data for three ZIKV-Fabs (ZV-2, orange; ZV-64, blue; and ZV-67, purple) in complex with the ZIKV EDIII (PDB: 5KVD, 5KVF, and 5KVG, respectively) guided resurfacing ZDIII-WT by phage display. (B) Cartoon of ZIKV E protein homodimer (PDB: 5JHM), color-coded by domain. Critical contact residues for mAbs ZV-2 and ZV-64 were identified in the ABDE sheet (orange spheres) and CC' loop (blue spheres) epitopes of ZDIII-WT and targeted for masking by mutagenesis to alanine. (C) Screen of reactivity profiles for rsZDIIIs mono-clonal phage toward ZIKV-mAbs (ZV-2, ZV-64, and ZV-67). Data from a single experiment, completed in duplicate, is plotted as (mean OD_{450}) ± standard deviation (SD). (D) rsZDIII phage reactivity toward ZV-mAbs determined by ELISA. Data from two experiments, completed in duplicate, is shown as half-maximal phage binding titer Log_{10} (EC_{50}). (E) Mutations in identified rsZDIIIs at targeted positions

in the ABDE sheet and CC' loop epitopes relative to WT. Mutation to alanine is indicated in red, with other amino acid substitutions in green.

Author Manuscript Author Manuscript Author Manuscript Author Manuscript

Author Manuscript Author Manuscript Author Manuscript Author Manuscript

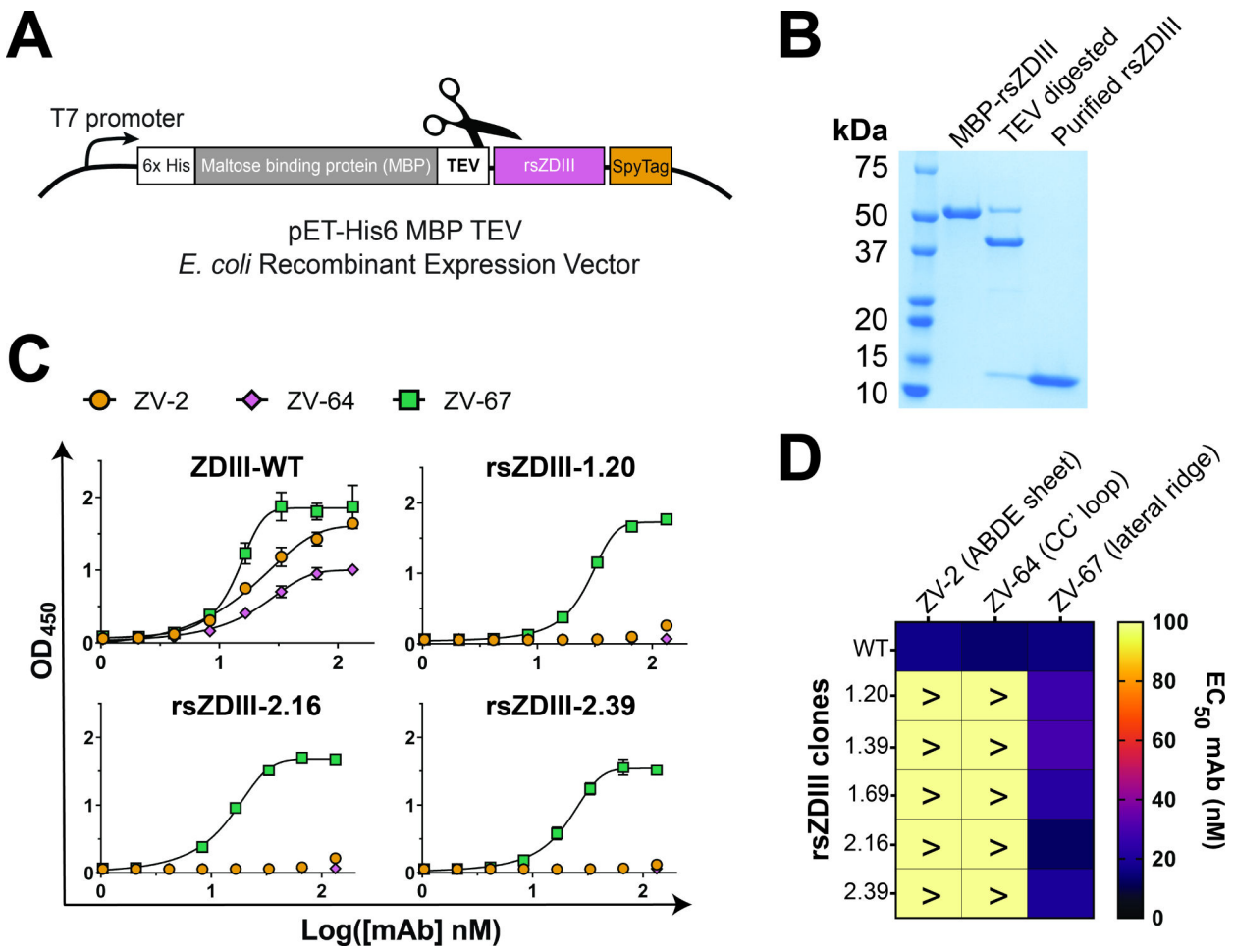

Figure 2. Expression and characterization of purified rsZDIIIs shows attenuated binding of ZV-mAbs to masked epitopes.

(A) Schematic representation of the bacterial expression vector used to produce soluble rsZDIIIs-SpyT as a fusion protein to MBP. A TEV cleavage site enables release and subsequent purification of soluble rsZDIIIs. (B) Two-step protein purification by Ni-NTA and anion exchange chromatography yields high purity, soluble rsZDIIIs. (C) Binding reactivity of ZV-mAbs (ZV-2, ZV-64, and ZV-67) to soluble rsZDIII variants determined by ELISA. Representative data from two independent experiments completed in triplicate are plotted as the (mean OD450) ± SD. (D) EC_{50} values for data plotted in panel (C).

Author Manuscript Author Manuscript Author Manuscript Author Manuscript

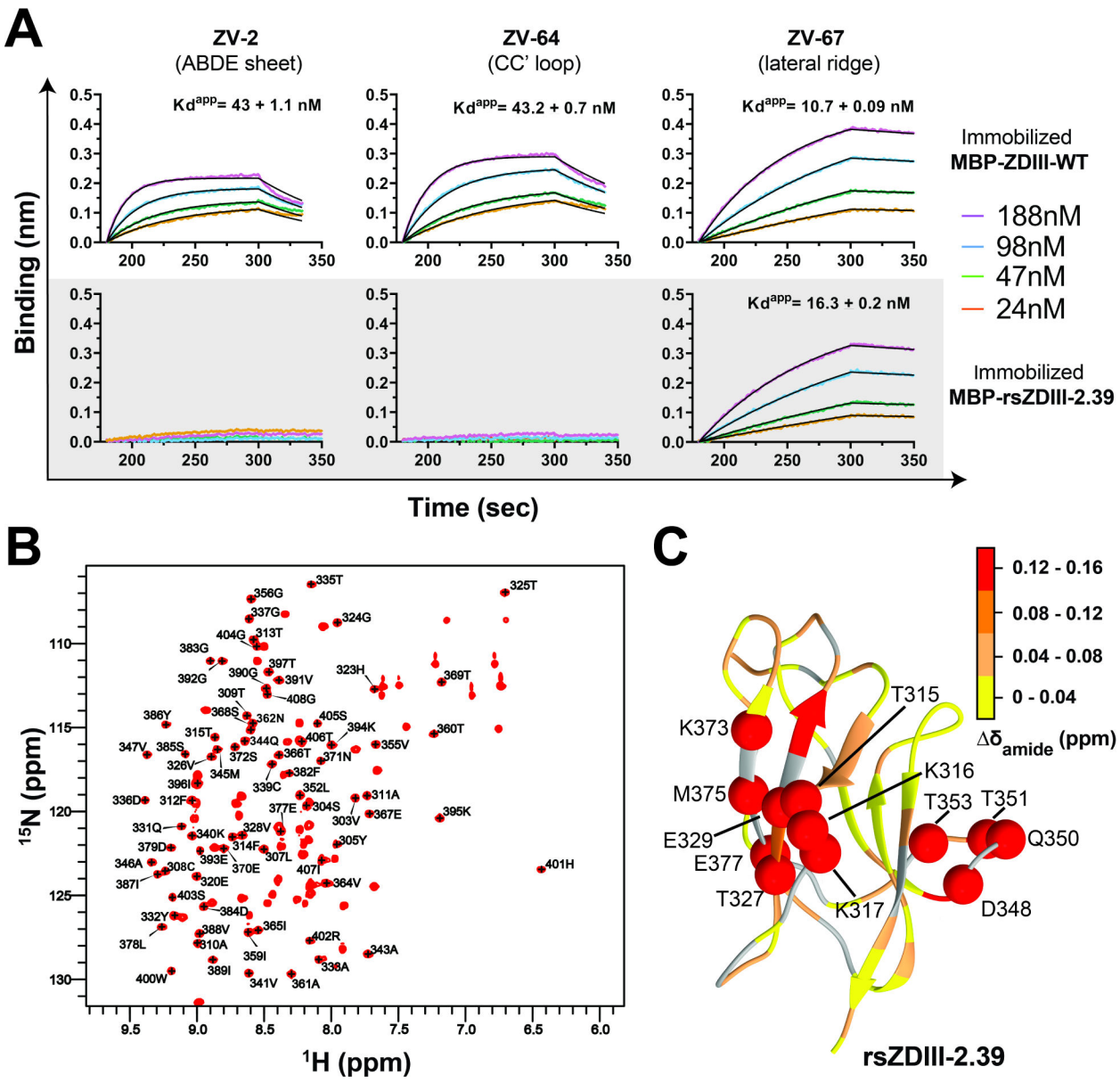

Figure 3. Biochemical and structural characterization of clone rsZDIII-2.39.

(A) Reactivity profiles for ZDIII-WT and rsZDIII-2.39 to ZIKV-mAbs (ZV-2, ZV-64, and ZV-67) as determined by BLI. Representative data from two independent experiments with consistent results. (B) HSQC plot of ^{1}H-^{15}N rsZDIII-2.39 assigned core residues. (C) Chemical shift differences between rsZDIII-2.39 and ZDIII-WT (BMRB 34167) molecules, presented as a structural projection onto ZDIII-WT (PDB: 5KVG).

Author Manuscript Author Manuscript Author Manuscript Author Manuscript

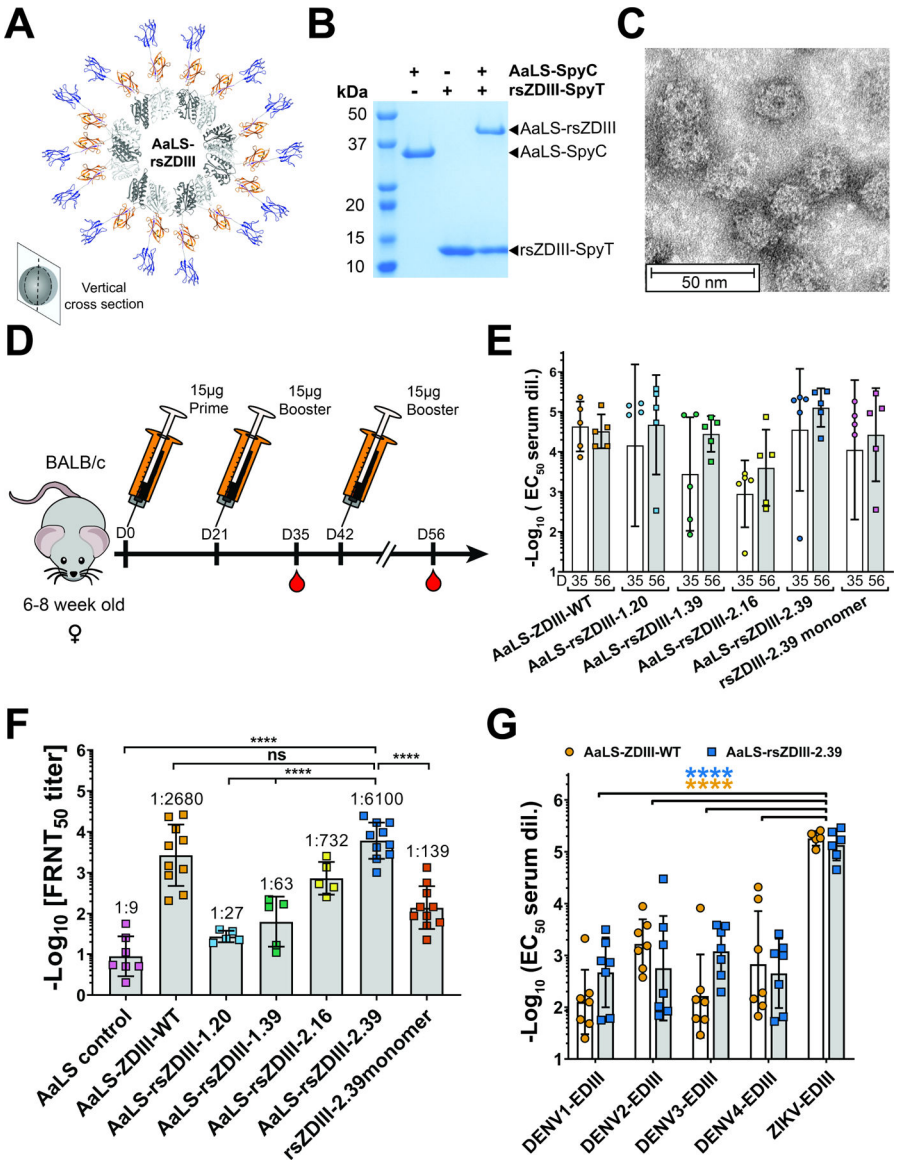

Figure 4. Generation and immunogenicity of Aquifex aeolicus Lumazine synthase (AaLS) nanoparticles displaying rsZDIIIs.

(A) Modelled structural cross-section of AaLS-rsZDIII nanoparticle (AaLS protomers shown in light/dark gray; SpyT/SpyC complex shown in orange; rsZDIII-2.39 shown in blue). (B) Generation of AaLS-rsZDIII nanoparticles by bio-coupling of AaLS-SpC with rsZDIIIs-SpT. SpyC and SpyT moieties spontaneously react to covalently associate. (C) Negative stain electron microscopy of AaLS-rsDIII-2.39 nanoparticle preparations, 50 nm scale bar shown for reference. (D) Mouse immunization and blood collection schedule. (E) D35 and D56 serum reactivity (n=5) for each immunogen group determined by ELISA. Data from a single experiment, performed in triplicate, shown as EC_{50} values for each animal, including $-Log_{10}$ (EC_{50} mean) ± SD for each group. (F) D56 serum FRNT neutralization titers for each immunization group. Data graphed as mean $FRNT_{50}$ values for each animal (n=5–10) from two independent experiments in triplicate, including Log_{10} ($FRNT_{50}$ mean) ± SD for the group. (G) Cross-reactivity of D56 sera elicited by AaLS-ZDIII-WT and

Author Manuscript Author Manuscript Author Manuscript Author Manuscript

AaLS-rsZDIII-2.39 against DENV1–4 EDIIIs. Data from two independent experiments in triplicate, shown as mean EC_{50} values for each animal (n=3), including $-Log_{10}$ (EC_{50} mean) ± SD. (FRNT neutralization and cross-reactivity analysis: 2-way ANOVA with Tukey's multiple comparisons test: *p< 0.05; **p<0.01; ***p<0.001; ****p<0.0001).

Author Manuscript Author Manuscript Author Manuscript Author Manuscript

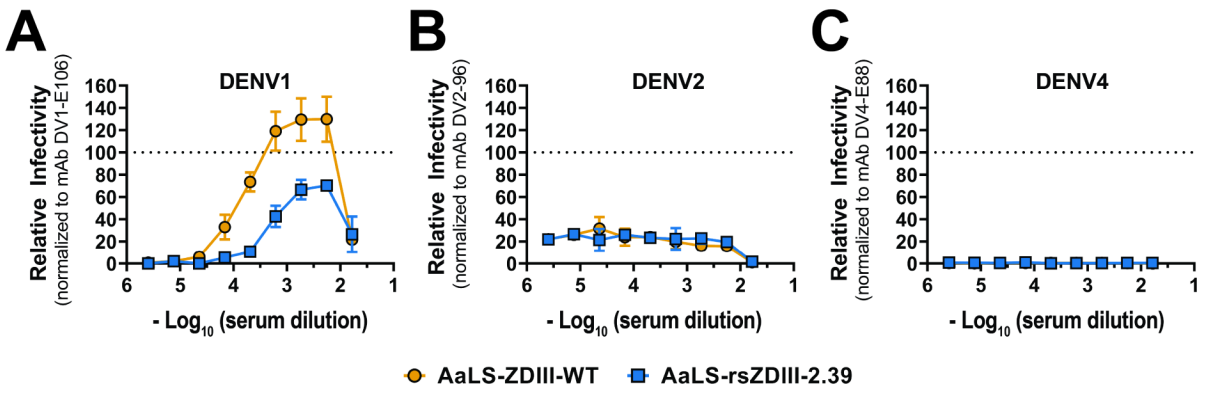

Figure 5. Antibody-dependent enhancement (ADE) assays of elicited serum.

Serial dilutions of pooled mouse sera were mixed with the indicated RVPs and incubated with Fcγ-receptor expressing K562 cells. Infected cells were quantified by flow cytometry. Dose-response curves for DENV1 (A), DENV2 (B) and DENV4 (C) RVPs are shown. Results are displayed relative to the maximum infectivity observed with a type-specific EDIII-reactive mAb run in parallel for each RVP. The dotted line is provided as a reference for normalization. Error bars indicate the range of duplicate technical replicates; data is representative of two independent experiments.

Author Manuscript Author Manuscript Author Manuscript Author Manuscript

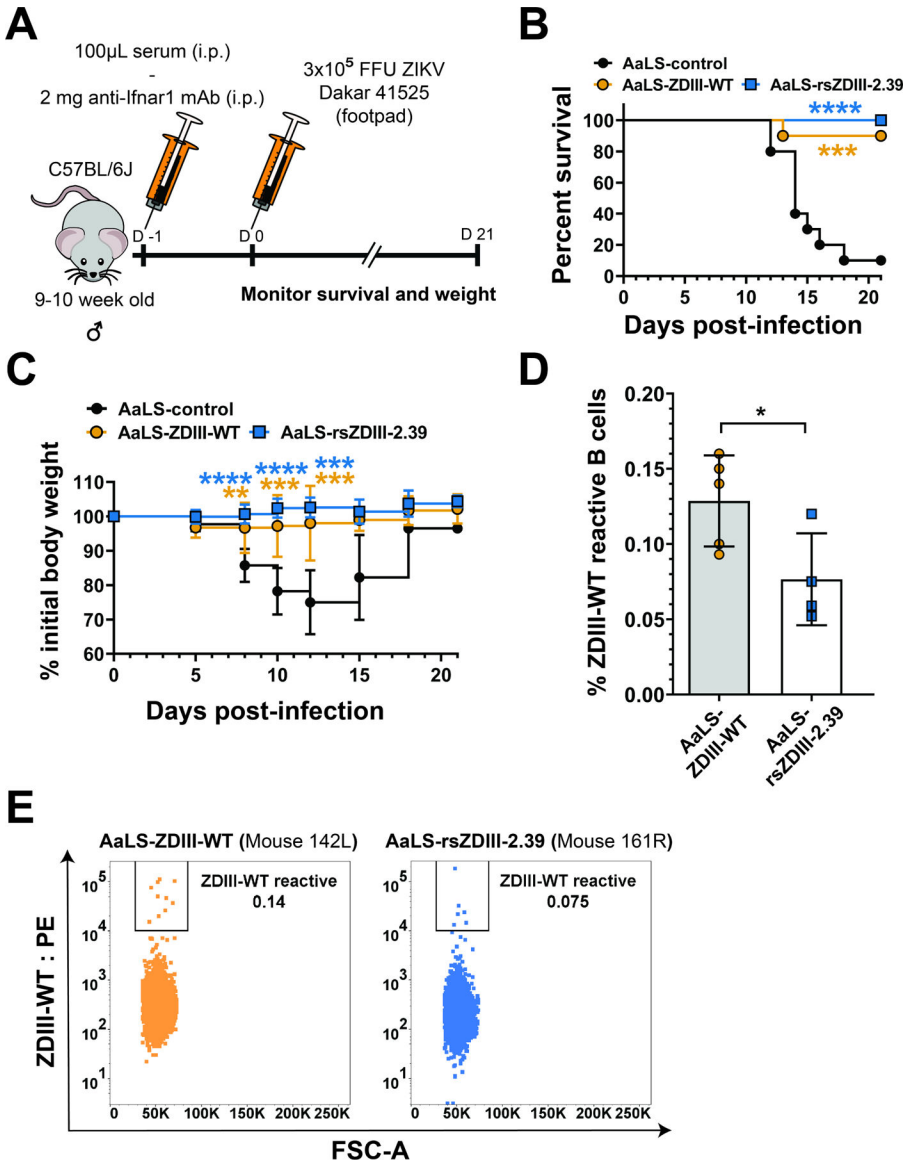

Figure 6. Serum elicited by resurfaced rsZDIII-2.39 protects mice in a lethal ZIKV challenge study with fewer ZDIII-WT antigen-reactive B cells.

(A) Viral challenge study design. 9- to 10-week-old C57BL/6J male mice in each test group were administered an anti-Ifnar blocking mAb and 100µL of D56 serum by intraperitoneal injection (i.p.). The next day (D0), mice were inoculated by subcutaneous injection in the footpad with 3×10^5 FFU of ZIKV Dakar 41525. Animals then were monitored for mortality and weight change for three weeks. (B) Survival following ZIKV infection as described in (A). Survival was analyzed using the log-rank Mantel-Cox test with a Bonferroni correction for 2 experiments (n = 10 mice per group; AaLS-ZDIII-WT, p = 0.0012; AaLS-rsZDIII-2.39, p < 0.0001). (C) Change in initial animal weight following ZIKV infection. Weights were analyzed by 2-way ANOVA with Sidak's post-test relative to the AaLS-control group; **p<0.01; ***p<0.001; ****p<0.0001. (D) Frequency of ZDIII-WT antigen-reactive $CD19^+$/ IgG^+ B cells in splenocytes from AaLS-rsZDIII-2.39 or AaLS-ZDIII-WT immunized animals were analyzed by flow cytometry, mean ± SD shown. Frequency of

antigen-reactive B cell was analyzed by unpaired t-test, *$p < 0.05$. (E) Representative dot plots of ZDIII-WT antigen-reactive B cell populations from a mouse in each immunization group.

Author Manuscript Author Manuscript Author Manuscript Author Manuscript

Author Manuscript Author Manuscript Author Manuscript Author Manuscript

Key resources table

REAGENT or RESOURCE	SOURCE	IDENTIFIER
Antibodies		
mAb ZV-2	Zhao et al., 2016	
mAb ZV-64	Zhao et al., 2016	
mAb ZV-67	Zhao et al., 2016	
mAb E60	Oliphant et al., 2006	
mAb DV1-E106	Shrestha et al., 2010	
mAb DV2–96	Sukupolvi-Petty et al., 2010	
mAb DV4-E88	Sukupolvi-Petty et al., 2013	
PE-Cy7 anti-mouse CD3	Biolegend	Cat# 100220
PE-Cy7 anti-mouse CD8a	Biolegend	Cat# 100722
PE-Cy7 anti-mouse F4/80	Biolegend	Cat# 123114
PE-Cy7 anti-mouse Gr-1	Biolegend	Cat# 108416
Pacific Blue anti-mouse CD19	Biolegend	Cat# 115523
FITC anti-mouse IgG	Biolegend	Cat# 406001
anti-FLAG mAb M2	Sigma-Aldrich	Cat# F3165–1MG
Horseradish peroxidase-conjugated anti-M13 antibody	Creative Diagnostics	Cat# CAB-655M
Horseradish peroxidase-conjugated protein	ThermoFisher	Cat# 101023
Horseradish peroxidase-conjugated goat anti-mouse IgG (H +L) antibody	ThermoFisher	Cat# 31430
anti-Ifnar1 mAb (MAR1–5A3)	Leinco technologies	Cat# I-401
Bacterial and virus strains		
ZIKV H/PF/2013	MS. Diamond	N/A
ZIKV Dakar 41525		N/A
M13KO7 helper phage	NEB	Cat# N0315S
E. coli CJ236	Lucigen	Cat# 06701–2
E. coli SS320	Lucigen	Cat# 60512–2
E. coli XL1-Blue	Agilent	Cat# 200228
E. coli BL21 Star (DE3)	ThermoFisher	Cat# C601003
Biological samples		
Immunized murine spleens	This paper	N/A
Chemicals, peptides, and recombinant proteins		
Biotinylated ZDIII-WT flow cytometry probe	This paper	N/A
AaLS protein nanoparticles	This paper	
Ammonium chloride (15N)	Cambridge Isotope Laboratories	Cat# NLM-467-PK
Critical commercial assays		

Author Manuscript Author Manuscript Author Manuscript Author Manuscript

REAGENT or RESOURCE	SOURCE	IDENTIFIER
ExpiCHO™ Expression System Kit	ThermoFisher	Cat# A29133
Gibson Assembly® Master Mix	NEB	Cat# E2611L
EZ-Link™ NHS-PEG4-Biotinylation kit	ThermoFisher	Cat# A39259
Experimental models: Cell lines		
Vero cells	ATCC	ATCC CCL-81
HEK-293T cells	ATCC	ATCC CRL-3216
Raji cells	ATCC	ATCC CCL-86
Experimental models: Organisms/strains		
BALB/C	Charles River Laboratories	Cat# 028
C57BL/6J	Jackson Laboratory	Cat# 000664
Oligonucleotides		
Alanine library primer #1 gccgccttcaccttcRCTRMARYTccggccgaaaccctgcatggcaccgtgRCTgtgGMAgtgcagtatgccggt	This paper	N/A
Alanine library primer #2 gcccagatggccgtgGMTatgSMARCTctgRCTccggtgggtcgcctg	This paper	N/A
Alanine library primer #3 agcaccgagaacagcRMAatgRYGctgGMActggatccgccgttc	This paper	N/A
Recombinant DNA		
pET-His6 MBP TEV cloning vector	S Gradia	Addgene29656
pET28a expression vector	Sigma-Aldrich	Cat# 69864
Software and algorithms		
Prism 8	GraphPad Software	www.graphpad.com/scientific-software/prism/
Bruker Topspin	Bruker Corp.	www.bruker.com/en/products-and-solutions/mr/nmr-software/topspin.html
NMRPIPE	Delaglio, 1995	
CcpNMR	Vranken et al., 2005	
FlowJo 10	Becton, Dickinson and Company	https://www.flowjo.com/solutions/flowjo
BioSpot	Immunospot	https://immunospot.com/plaque-colony-counting
Octet Systems	Sartorius	https://www.sartorius.com/en/products/protein-analysis/octet-systems-software
Other		
Nickel nitrilotriacetic acid (Ni-NTA) resin	Goldbio	Cat# H-355–100
Addavax immunization adjuvant	Invivogen	Cat# vac-adx-10

REAGENT or RESOURCE	SOURCE	IDENTIFIER
TrueBlue reagent	Seracare	Cat# 5510–0030
Strepavidin-PE	Life technologies	Cat# S21388

Author Manuscript
Author Manuscript
Author Manuscript
Author Manuscript